Department of Clinical Research and Veterinary Public Health Division of Veterinary Pharmacology and Toxicology Vetsuisse Faculty, University of Bern

Director Head of Institution Prof. Dr. med. vet. Meike Mevissen

Scientific supervision was provided by Dr. Angélique Ducray Prof. Dr. med. vet. Meike Mevissen

Neuronal health in a wireless world: the role of PARP1 and 5G non-ionizing radiation in neuronal development

Inaugural Dissertation

to be awarded the Doctoral Degree of the Vetsuisse Faculty, University of Bern

submitted by

Alexander Baumgartner

Veterinarian from Hasle b. Burgdorf BE

2024

This work is licensed under CC BY 4.0. To view a copy of this license, visit https://creativecommons.org/licenses/by/4.0/

Approved by the Vetsuisse Faculty a from Prof. Dr. med. vet. Meike Mevissen	s inaugural dissertation on proposal
Prof Dr. Marco Alves	
Bern,	Dean of the Vetsuisse Faculty University of Bern



Contents

Contents	4
Summary	5
_ist of abbreviations	6
ntroduction	8
Materials and methods	11
Plasmid Design	11
Cell culture	12
Generating monoclonal PARP1 knockout cells	13
Transfection	13
Cell sorting	13
Verification of pluripotency	15
Differentiation into dopaminergic neurons	15
5G NR FR1 RF-EMF Exposure	16
Western blotting	18
Immunofluorescence	19
Statistical analysis	20
Results	21
Validation of the PARP1-KO	21
Validation of pluripotency	21
PARP1 protein levels	23
Neuronal phenotype	24
TUJ1 and TH protein levels	24
MAP2 protein levels	27
Synaptic plasticity	30
SYP protein levels	30
αSyn protein levels	31
Glial marker	32
S100β protein levels	32
Discussion	34
Conclusion	40
References	41
Acknowledgements	45
Declaration of independance	46

Vetsuisse Faculty University of Bern 2024

Alexander Baumgartner

Division of Veterinary Pharmacology and Toxicology

Contact: regula.aebi@unibe.ch

Neuronal health in a wireless world: the role of PARP1 and 5G non-

ionizing radiation in neuronal development

Summary

The fifth generation (5G) of wireless technology, operating within non-ionizing

radiofrequency electromagnetic (RF-EMF) spectrum, has transformed connectivity

while raising concerns about potential health effects, including neurodegeneration.

Previous findings suggest that RF-EMF may impact neuronal function, oxidative stress,

and DNA damage, potentially contributing to neurodegenerative diseases.

In this study, the role of poly (ADP-ribose) polymerase 1 (PARP1), a key enzyme in

DNA repair, but also a player in neuronal development and neurodegeneration was

investigated. In addition, effects of 5G radiation were studied in human induced

pluripotent stem cells (iPSCs) under development to dopaminergic neurons.

PARP1 knockout (KO) monoclonal human iPSCs were successfully generated using

CRISPR/Cas9. Both KO and wild-type (WT) cells were exposed to 5G RF-EMF during

the induction phase, and protein analyses regarding phenotype neuronal maturity,

synaptic plasticity, and appearance of astrocytes were performed after differentiation

and maturation.

The results showed a time-dependent increase in all investigated neuronal markers

over time, indicating neuronal development. PARP1-KO significantly enhanced the

dopaminergic phenotype. RF-EMF exposure resulted in alterations of the synaptic

markers.

These findings highlight PARP1's role in dopaminergic differentiation and suggest

limited effects of RF-EMF on neuronal development especially in synaptic plasticity.

Keywords: PARP1, CRISPR/Cas9, human iPSC, dopaminergic neurons,

radiofrequency electromagnetic fields, 5G

5

List of abbreviations

5G 5th generation

AD Alzheimer's disease

ADP adenosine diphosphate

AF alexa fluor αSyn α-synuclein

Cas9 CRISPR associated Protein 9

CNS central nervous system

CRISPR clustered regularly interspaced short palindromic repeats

DAPI 4',6-diamidino-2-phenylindole

DIV days in vitro

DNA deoxyribonucleic acid

DPBS dulbecco's phosphate-buffered saline

EDTA ethylenediaminetetraacetic acid

EEG electroencephalography

FACS fluorescence-activated cell sorting
FOEN Federal Office for the Environment

FR1 frequency range 1

GCDR gentle cell dissociation reagent

GFP green fluorescent protein

gRNA guide ribonucleic acid
HRP horseradish peroxidase
IF immunofluorescence

IgG immunoglobulin G

iPSC induced pluripotent stem cells

-ir immunoreactive

KO knockout

LB Luria-Bertani

LDS lithium dodecyl sulfate

MAP2 microtubule associated protein

MHz megahertz

NAD+ nicotinamide adenine dinucleotide

NIR non-ionizing radiation

NR new radio

P passage

PAR poly (ADP-ribose)

PARP1 poly (ADP-ribose) polymerase 1 PARP2 poly (ADP-ribose) polymerase 2

PCR polymerase chain reaction

PD Parkinson's disease
PFA paraformaldehyde
PLO poly-L-ornithine

PVDF polyvinylidene difluoride

RF-EMF radio frequency electromagnetic field

ROCKi ROCK inhibitor Y-27632 ROS reactive oxygen species

RT room temperature

S100 S100 calcium-binding protein B

SAR specific absorption rate

SEM standard error of the mean

Shh human recombinant sonic hedgehog

SMADi SMAD inhibitor

SSEA5 stage specific embryonic antigen-5

SYP synaptophysin

TH tyrosine hydroxylase

TP time pointTRA-1-60 podocalyxinTUJ1 βIII-tubulin

W watts

WB western blot

WHO World Health Organization

WT wildtype

Introduction

The fifth generation (5G) of wireless mobile technology, known as 5G NR (New Radio), has introduced a new era of high-speed internet and enhanced connectivity since its extensive rollout in 2019. Operating within the non-ionizing radiation (NIR) spectrum, specifically radio frequency electromagnetic fields (RF-EMF) and frequency range 1 (FR1) (<6 GHz), the 5G technology enables higher data transfer rates and low latency essential for modern applications (IBM 2024; MIT Sloan 2020). Despite these advancements, concerns persist regarding potential health impacts of RF-EMF including 5G, one being their possible role in promoting or accelerating neurodegenerative diseases and their progression. Although substantial research on RF-EMF at lower frequencies has been performed, studies focusing on effects of NIR in the 5G RF-EMF context remain limited.

Current research on the impact of RF-EMF related to neurodegeneration showed different findings that are not conclusive. Some studies suggest that exposure to RF-EMF could potentially impair neuronal morphology and function. For instance, it was demonstrated in an in vitro model that RF-EMF exposure (13.56 MHz, 80 W) increased the permeability of the blood-brain barrier, highlighting a potential impact on its protective function (Senturk et al. 2022). Additionally, RF-EMF exposure (900 MHz, SAR of 2 W/kg) was shown to increase electroencephalography (EEG) spindle frequency power during sleep, indicating alterations in neuronal activity (Schmid et al. 2012). Memory impairments were demonstrated in mice exposed to intermediate frequency magnetic fields (7.5 kHz), with behavioral tests revealing disruptions in cognitive performance (Kumari et al. 2017). These findings suggest that RF-EMF exposure can negatively affect learning and memory. Similarly, it was reviewed that RF-EMF might interfere with neurological processes, potentially contributing to cognitive deficits through mechanisms such as altered neuronal activity and oxidative stress (Schuermann and Mevissen 2021). The role of oxidative stress after RF-EMF exposure was further emphasized, identifying it as a key factor leading to cellular damage and inflammation (Bandara and Weller 2018). The imbalance between reactive oxygen species (ROS) production caused by RF-EMF and antioxidant defenses may contribute to neurodegeneration and cognitive decline (Bandara and Weller 2018). A study on the possible effects of RF-EMF on male reproductive health also summarized evidence for its role in DNA damage, chromosomal aberrations, and

oxidative stress (Kaur et al. 2023). Oxidative stress and mitochondrial dysfunction were shown to contribute to the development of neurodegenerative disorders including Parkinson's disease (PD) and Alzheimer's disease (AD) (Houldsworth 2024; Knott et al. 2008; Korovesis, Rubio-Tomás, and Tavernarakis 2023; Teleanu et al. 2022). However, the findings are controversial, and the World Health Organization (WHO) has reviewed the potential health effects of RF-EMF, including their impact on neurological outcomes. As of their latest assessments, the WHO states that current evidence does not confirm any adverse health effects from exposure to RF-EMF, such as those emitted by mobile phones and wireless networks. Specifically, they state that there is no conclusive evidence linking RF-EMF exposure to neurological disorders or cognitive impairments (WHO 2020). Regulatory bodies and health organizations, like the WHO and the Federal Office for the Environment (FOEN) in Switzerland continue to monitor research to provide guidelines based on the most current scientific evidence following the precautionary principle (FOEN 2024). Ongoing studies aim to elucidate the potential risks, ensuring that the deployment of such technology proceeds with a thorough understanding of its health impacts. As the scientific community continues to explore these effects, it remains crucial to balance technological progress with public health considerations.

RF-EMF exposure was shown to induce ROS formation (Schuermann and Mevissen 2021), leading to DNA damage, which was demonstrated to be involved in the development and progression of neurodegenerative diseases (Aslan et al. 2020, H. Zhao et al. 2022). Recent studies have linked poly (ADP-ribose) polymerase 1 (PARP1) to neuronal development and neurodegenerative diseases (Arruri et al. 2021). PARP1 is the most studied member of the PARP family, which includes 17 proteins capable of transferring mono (ADP-ribose) or poly (ADP-ribose) (PAR) units to target proteins (Mao and Zhang 2022). This family shares a conserved catalytic domain that facilitates these modifications (Mao and Zhang 2022). PARP1 and PARP2 are particularly important, with PARP1 accounting for 85-90% of the activity, engaging in numerous cellular processes such as DNA repair, maintaining genomic stability, cell proliferation, differentiation, and apoptosis (Mao and Zhang 2022; Park et al. 2020; Pazzaglia and Pioli 2019). The essential role of PARP1 in a wide range of physiological processes, including development, immune response, nervous system function, aging, and cancer progression was reviewed by Krishnakumar and Kraus (2010). PARP1 was shown to be integral to developmental programming, where it regulates the expression of multiple genes in embryonic stem cells, thereby influencing cellular differentiation and driving developmental processes (Krishnakumar and Kraus 2010). In addition to its role in stem cell biology, PARP1 has been shown to play a pivotal part in the development of neurons (Nelson et al. 2021). PARP1 is crucial for brain development, regulating Cajal-Retzius cells, neuronal density, and neural precursor adhesion through migration-related genes (Nelson et al. 2021). Furthermore, PARP1's involvement in the development and progression of neurodegenerative diseases was demonstrated, emphasizing its critical involvement in the pathophysiology of neurological disorders such as AD and PD (Mao and Zhang 2021; Thapa et al. 2021). The potential of targeting PARP1 as a therapeutic strategy for neurodegenerative diseases has been underlined, with its role in neurodegeneration described as both protective and harmful (Mao and Zhang 2022; Thapa et al. 2021). PARP1 was reported to help maintain genomic integrity by repairing damaged DNA (Azarm and Smith 2020). However, overactivation of PARP1, often triggered by excessive DNA damage in neurodegenerative conditions, can lead to cellular energy depletion and trigger cell death pathways (Arruri et al. 2021). This overactivation is known to consume large amounts of cellular nicotinamide adenine dinucleotide (NAD+), which is essential for cellular metabolism and energy production. Depletion of NAD+ results in cellular energy crisis and eventually lead to cell death, a process referred to as parthanatos (Huang et al. 2022; Liu et al. 2022). During the early phase in the development of neurodegenerative diseases, controlled PARP1 activation has been shown to help address mild DNA damage and maintain brain homeostasis. However, at later stages, excessive PARP1 activation, due to severe DNA damage, worsened the disease condition. (Hu et al. 2023)

This study aimed to examine the impact of 5G NR FR1 radiation on the early development of dopaminergic neurons, utilizing both wildtype (WT) and PARP1 knockout (PARP1-KO) cells. The objective was to assess the role of PARP1 in neuronal differentiation and investigate potential effects of 5G NR FR1 exposure. This research is crucial for understanding the influence of 5G RF-EMF on neuronal development and the role of PARP1.

Materials and methods

Plasmid Design

To create PARP1-knockout (KO) cells, the CRISPR/Cas9 technology was used. The pSpCas9(BB)-2A-Puro (PX495) V2.0 (Addgene, USA) vector was used for cloning of the respective guide RNAs (gRNAs). This plasmid contains an ampicillin resistance for bacterial selection and a puromycin resistance for cell selection.

Three different gRNA (Table 1) were designed using the CHOPCHOP web tool (Labun et al. 2019). While gRNA1 targets exon 2 on the human PARP1 (hu-PARP1) gene, gRNA2 targets exon 3 and gRNA3 targets exon 1. All three exons code for the DNA-binding domain of the protein.

To clone the gRNAs into the plasmid, the golden gate cloning method was used. Linearization of the plasmid was done using BbsI-HF® restriction enzyme (New England Biolabs, USA).

Afterwards, the plasmid containing the gRNA was transformed in NEB® stable competent *Escherichia coli* (New England Biolabs, USA). Incubation on agar plates containing 100 µg/mL ampicillin was performed for selection, and after 24 hours eight colonies were randomly picked from each plate to perform an overnight culture in Luria-Bertani (LB)-medium also containing 100 µg/mL ampicillin. To verify that the gRNAs were correctly integrated, Sanger sequencing was performed (Microsynth AG, Switzerland).

Table 1: gRNAs used for cloning

	exon	sequence
gRNA1	exon 2	TTCTAGTCGCCCATGTTGA
gRNA2	exon 3	AAGTACGTGCAAGGGGTGTA
gRNA3	exon 1	CGAGTCGAGTACGCCAAGAG

Cell culture

The cells used for this work were human induced pluripotent stem cells (hu-iPSC) of the cell line IMR90 Clone #4, which were previously purchased from WiCell, USA.

Unless stated otherwise, all the reagents used for cell culture were purchased from STEMCELL Technologies, Switzerland.

iPSCs were expanded in T25 flasks (Corning, USA) coated with Vitronectin XF, utilizing mTeSR™1 medium, which is formulated to support the growth and pluripotency of human pluripotent stem cells in a feeder-free culture system (STEMCELL Technologies 2024). The medium was replaced daily with mTeSR™1, while over the weekends, the cells were maintained in mTeSR™ Plus for two days. The cells were incubated at 37°C and 5% CO₂ until they reached 80-90% confluency. Passage was performed using Gentle Cell Dissociation Reagent (GCDR) to detach the cells, ensuring minimal cellular stress and preserving the integrity of the colonies. Figure 1 illustrates the workflow followed to obtain monoclonal PARP1-KO cells. These cells were subsequently differentiated into dopaminergic neurons.

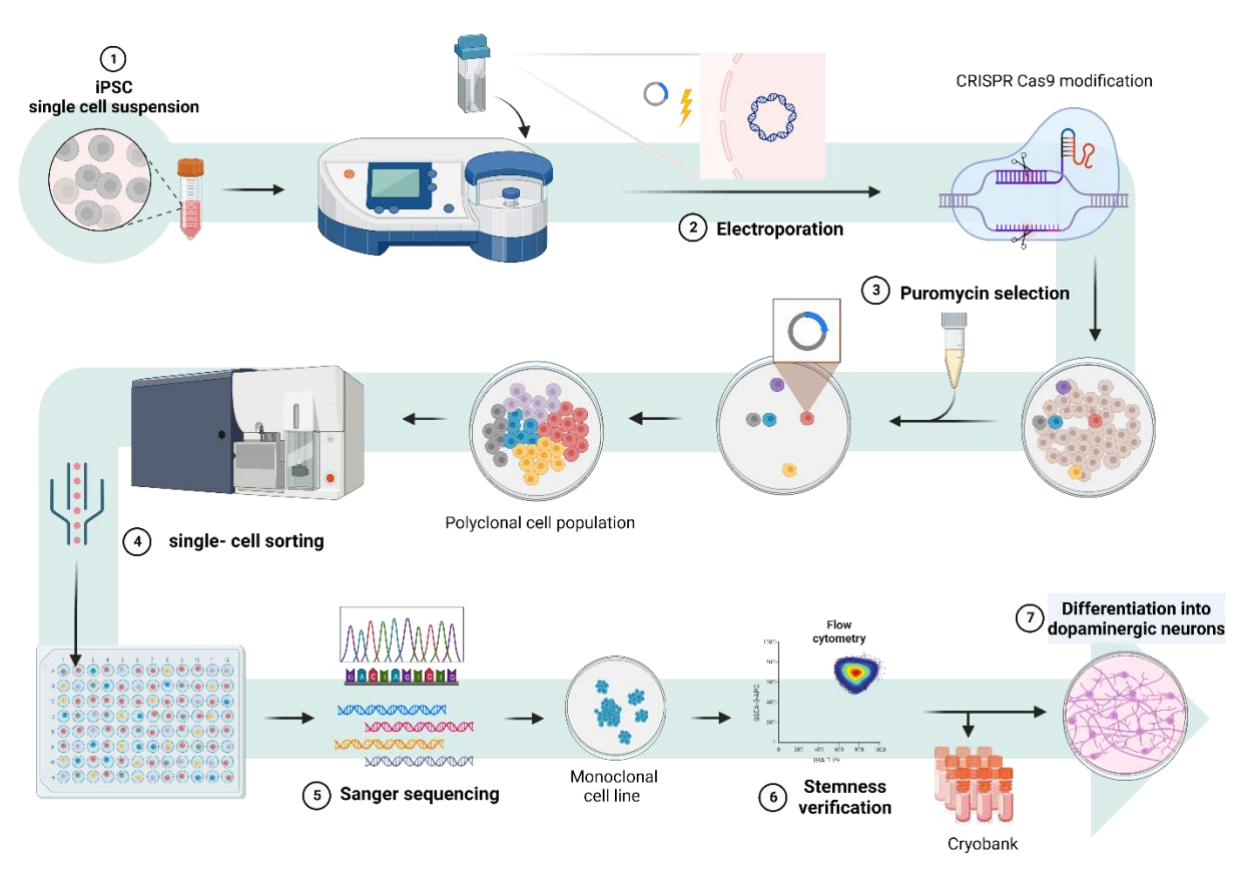


Figure 1: Illustration of the timeline of generating PARP1-KO cells. Adapted from Weber et al. (2023)

Generating monoclonal PARP1 knockout cells

Transfection

iPSCs were transfected separately with plasmids contain one of the three different gRNAs (Table 1) and the LRG2.1_Puro Plasmid (Addgene, USA), which contains a green fluorescent protein (GFP) to assess transfection efficiency resulting in four separate transfections.

To transfect iPSCs with plasmids containing the gRNAs, the cells were first harvested using ACCUTASETM for 8 minutes at 37°C to achieve a single cell suspension. For each transfection, 800,000 cells were used along with 5 μ g of vector containing the corresponding gRNA. Transfections were carried out using the 4D NucleofectorTM X Unit (Lonza, Switzerland) with 100 μ L NucleovettesTM (Lonza, Switzerland) in combination with the P3 Primary Cell Solution (Lonza, Switzerland) and the program CA-137.

Following electroporation, the transfected cells were immediately seeded into 24-well plates coated with Vitronectin XF. The cells were then cultured at 37°C and 5% CO₂ with daily medium change in mTeSR $^{\text{TM}}$ Plus medium supplemented with 10 μ M ROCK inhibitor Y-27632 (ROCKi) and 10% CloneR $^{\text{TM}}$ 2 to promote survival and recovery post-transfection. In addition, iPSC wildtype (WT) electroporated without a vector were seeded under the same conditions to obtain a negative control.

On day *in vitro* (DIV) 1 after electroporation a full medium change was done using mTeSR™ Plus medium without ROCKi and CloneR™2. Puromycin (1 µg/mL) dihydrochloride (Sigma Aldrich, Germany) was added to the medium on DIV2 to ensure the survival of only cells that successfully incorporated and expressed the plasmid. The puromycin selection was done for 48 hours and after that the mTeSR™ Plus medium was changed daily without any additives. Surviving cells were expanded to a confluency of 80-90% and then passaged to 6-well plates using GCDR to dissociate the cells. The wells of the 24-well plates passaged to 6-well plates were randomly picked.

Cell sorting

As soon as the colonies in the 6-well plates reached a confluency of 80-90%, they were sorted using fluorescence-activated cell sorting (FACS). For this purpose, the cells

were dissociated into a single-cell suspension using ACCUTASE™ and transferred into Falcon® Round-Bottom tubes in which they were stained with 1 µg/mL 4',6-diamidino-2-phenylindole (DAPI; Sigma-Aldrich, Germany). DAPI staining was used to selectively exclude dead cells, as it penetrates only cells with compromised membranes, ensuring that only viable, DAPI-negative cells were sorted. FACS was performed by the 'Flow Cytometry and Cell Sorting Core Facility' of the Department for BioMedical Research (Bern, Switzerland). One DAPI negative cell was sorted into each well of a 96-well plate. The cells were then incubated for 48 hours in eTeSR™ medium with 10% CloneR™2 and penicillin [100 U/mL]-streptomycin [100 µg/mL] (Thermo Fisher Scientific, Switzerland) at 37°C and 5% CO₂. The medium was changed every other day. Once the cell colonies were confluent, 24 colonies were randomly selected and passaged in 24-well plates. For passaging, GCDR and eTeSR™ medium with 10% CloneR™2 were used but at DIV 4 the medium was changed to mTeSR™1. After a further passage in 6-well plates, where the colonies were also randomly selected, the cells were transferred into T25 flasks as soon as they were confluent. During this passage, a portion of the cells was used to obtain DNA. About 50% of the cells were passaged and about 50% were used for DNA extraction. The cells in the T25 flasks were further expanded and then frozen in liquid nitrogen using mFreSR™ freezing medium. The DNeasy® Blood & Tissue Kit (Qiagen, Germany) was used for DNA extraction according to the manufacturer's protocol. The DNA obtained was then amplified by polymerase chain reaction (PCR) at an annealing temperature of 60°C and 35 cycles. The primers used for amplification are presented in table 2. To purify the PCR product the Exo-CIP™ Rapid PCR cleanup KIT (New England Biolabs, USA) was used. The purified PCR products were sent to Microsynth AG, Switzerland for sequencing. If sequencing confirmed a base insertion that resulted in a frameshift, the corresponding gRNA was selected for subsequent cell transfection.

Table 2: Primers used for amplification

	primer	sequence
gRNA1	FW-Primer 5'-3'	TGTCCTCCTTTCACAGATAAG
griva	RV-Primer 5'-3'	CCAGTATGTACACACCTGTCACT
gRNA2	FW-Primer 5'-3'	TGTTGAGATGAGCATTGCTGT
gKNAZ	RV-Primer 5'-3'	GTATCTGGTCAATACTAATGTC
gRNA3	FW-Primer 5'-3'	AATCTATCAGGGAACGGCGGT
gKNAS	RV-Primer 5'-3'	AGCCTTCCCGGACACAGTTAA

Verification of pluripotency

Before differentiating the cells into dopaminergic neurons, pluripotency was verified by flow cytometry. For this purpose, cells were first incubated with 0.02% Ethylenediaminetetraacetic Acid (EDTA) in Gibco™ Dulbecco's Phosphate-Buffered Saline (DPBS) (Thermo Fisher Scientific, USA) (0.5 mM) for 3 minutes followed by a second incubation with ACCUTASE™ for 8 minutes to produce a single cell suspension. Both, the incubation with EDTA/DPBS and with ACCUTASE™ were performed at 37°C and 5% CO₂. To inactivate ACCUTASE™, mTeSR™1 complete medium was added. This was followed by centrifugation at 280 g and room temperature (RT) for 5 minutes. After the resulting cell pellet was resuspended with DPBS (Thermo Fisher Scientific, USA), 800,000 KO and 800,000 WT cells were equally divided into two tubes each. The conjugated antibodies TRA-1-60-PE (Podocalyxin; STEMCELL Technologies, Switzerland) and SSEA5-APC (Stage-Specific Embryonic Antigen-5; STEMCELL Technologies, Switzerland) were used for staining. The antibodies were diluted 1:50 in CellWASH (BD Biosciences, USA). After another centrifugation at 280 g at 4°C for 8 minutes, the cell pellet was resuspended with 100 µL of the antibody solution and incubated for 15 minutes. Subsequently, the cells were centrifuged again for 8 minutes at 4°C and 280 g and then resuspended with 250 µL CellWASH (BD Biosciences, USA) and filtered through 35 µm cell stainer cap of Falcon® round-bottom tubes. Flow cytometry was performed with Cytek® Aurora (Cytek® Bioscience, USA). Pluripotency was confirmed when at least 80% of the cells were positive for SSEA5 and TRA-1-60.

Differentiation into dopaminergic neurons

For the generation of dopaminergic neurons, iPSC PARP1-KO and iPSC WT were first induced into neural progenitor cells (NPCs) using the STEMdiff™ SMADi Neural Induction Kit (STEMCELL Technologies, Switzerland). For this purpose, the cells were seeded on poly-L-ornithine (PLO) [15 μg/mL]-laminin [10 μg/mL] (Sigma-Aldrich, Germany) coated tissue culture treated 6-well plate (TPP Techno Plastic Products AG, Switzerland) at a density of 800,000 cells per well. After 6-8 days, with daily medium changes, and a cell density of 80-90%, the cells were dissociated into a single-cell suspension using ACCUTASE™ and passaged (P1) with the same density as they were seeded. Two further passages (P2 and P3) were performed in the same way. The cells were radiated with RF-EMF at DIV3-6 after P2 (see below). After the third passage

(P3), the cells were differentiated into midbrain neurons using the STEMdiff™ Midbrain Neuron Differentiation Kit according to the manufacturer's protocol (STEMCELL Technologies, Switzerland). On the first day after P3, the medium was changed to STEMdiff™ Midbrain Neuron Differentiation Medium supplemented with 200 ng/mL human recombinant Sonic hedgehog (Shh), which in turn was changed daily. The differentiation phase lasted 6-8 days and the cells were passaged as soon as they reached 80-90% confluence. In addition to being passaged, the cells were analyzed after differentiation (time point 1) by Western blot (WB) and immunofluorescence (IF) (see below). After the fourth passage (P4), the medium was changed to STEMdiff™ Midbrain Neuron Maturation Medium. Maturation was maintained for two weeks, with half of the medium being changed every 2-3 days. After two weeks of maturation (time point 2), the cells were also analyzed by WB and IF (see below). To ensure reproducibility, four independent runs with the exact same conditions were performed.

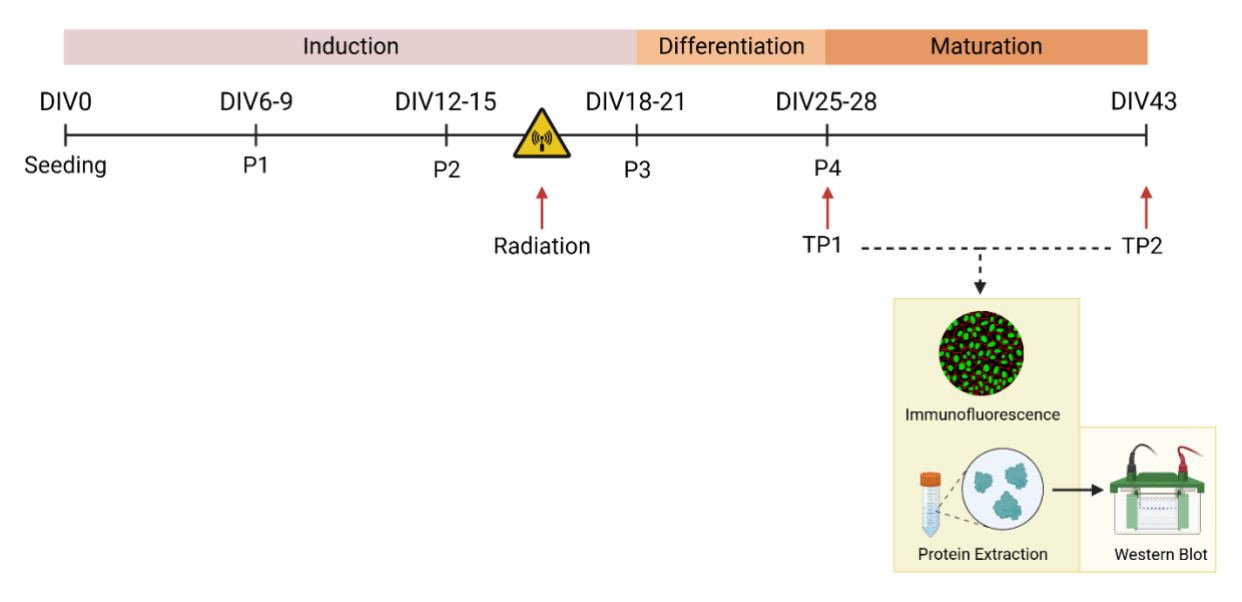


Figure 2: Illustration of the development of hu-iPSC-derived dopaminergic neurons. DIV = days *in vitro*, P = passage, TP1 = time point 1 (after differentiation), TP2 = time point 2 (after maturation). Created with BioRender.com

5G NR FR1 RF-EMF Exposure

Radiation of the cells was done during the induction phase in the development toward dopaminergic neurons. The sXc1950 system (IT'IS Foundation, Switzerland) was used to expose the cells to 5G NR FR1 radiation. Table 3 provides the characteristics of the exposure system, the dosimetry data, and the 5G NR FR1 RF-EMF signals used in this study.

Table 3: Physical properties of simulated 5G mobile communication signal (FR1) generated by an in vitro RF-EMF exposure system

Parameter	Signal value		
Carrier Frequency	1950 MHz ^a		
Bandwith	50-100 MHz		
Modulation 5G	OFDM ^b		
Sub-carrier spacing	15-30 kHz ^c		
Symbol Rate	14-28 kSps ^d		
Slot lenght	1 ms ^e		
Access method	TDD ^f , FDD ^g		

^aMHz (Megahertz), ^bOFDM (Orthogonal Frequency Division Multiplex),

The design of the system includes two waveguides. Each of these waveguides has space for six Petri dishes, allowing the simultaneous exposure of multiple samples. Three Petri dishes containing WT cells and three Petri dishes containing PARP1-KO cells were placed in each chamber, with the dishes randomly distributed between the two waveguides. The system randomly selects one waveguide for RF-EMF exposure, while the other waveguide is sham exposed, ensuring that the experiments can be conducted as a double-blind study. In this study, four different cell conditions were used, namely: WT sham-exposed, WT RF-EMF-exposed, PARP1-KO sham-exposed and PARP1-KO RF-EMF exposed.

The cells were radiated for 33 hours with an ON/OFF cycle of 10 minutes on and 10 minutes off, achieving an expected specific absorption rate (SAR) level of 3.5 W/kg. The highest possible SAR level was chosen that does not cause an increase in temperature above 37°C ± 0.1°C. The temperature was monitored constantly, and in case a temperature increase above the set limits happens, the experiment is immediately terminated. Additionally, the waveguides ventilation system ensured optimal temperature regulation throughout the exposure period, maintaining the temperature.

ckHz (kilohertz), dkSps (kilosample per second), emms (milliseconds),

^fTDD (Time Division Duplex), ^gFDD (Frequency Division Duplex)

Western blotting

WB analysis was performed to assess protein expression across the four different conditions (WT sham-exposed, WT RF-EMF-exposed, PARP1-KO sham-exposed and PARP1-KO RF-EMF-exposed) and two different time points, namely after differentiation and after maturation (Figure 2). To dissociate the cells, ACCUTASE™ was used followed by centrifugation at 100 g for 5 minutes at RT. The resulting cell pellets were resuspended in a lysis buffer (30 mM Tris-HCl (Sigma-Aldrich, USA), 1.5 mM MgCl2 (Merck, Germany), 10 mM KCl (Merck, Germany), 20% Glycerol (Sigma-Aldrich, USA), 1% Triton X-100 (Fluka Chemika, Switzerland)) containing a protease/phosphatase inhibitor cocktail (Thermo Fisher Scientific, Switzerland) at a dilution of 1:100. After an incubation time of 5 minutes on ice, another centrifugation step at 1000 g for 5 minutes at 4°C was applied.

The obtained lysate was then measured for protein concentration using NanoDrop™ Eight Spectrophotometer (Thermo Fisher Scientific, Switzerland). For this purpose, 10 µL of lysate was added to 150 µL of Pierce protein assay reagent (Thermo Fisher Scientific, Switzerland) and incubated in the dark for 5 minutes. The remaining lysates were mixed with 4X lithium dodecyl sulfate (LDS)-sample buffer (Witec, Switzerland) in a ratio of 3:1 and heated for 5 minutes at 95°C. Samples were stored at -20°C subsequently.

For protein separation 10 µg of each sample was loaded onto pre-cast 10% or 12% sodium dodecyl sulfate polyacrylamide gels (SDS-PAGE; SurePAGE Bis-Tris, Witec, Switzerland), separated by electrophoresis. and then transferred onto polyvinylidene difluoride (PVDF) membranes (Bio-Rad Laboratories, USA).

The membranes were blocked using 1X phosphate buffered saline (PBS) (pH 7.4), 0.2% Tween®20 (Sigma-Aldrich) and 5% non-fat milk powder solution (Migros, Switzerland) for 2 hours at room temperature (RT) with constant agitation. After the blocking, membranes were incubated with primary antibodies (Table 4) diluted in blocking solution over night at 4°C. Between the incubation with primary- and the incubation with HRP-conjugated secondary antibodies (Table 4) a washing step of four times 10 minutes with PBS-Tween®20 0.2% was carried out. After the incubation with secondary antibody for 2 hours at RT and another washing sequence of four times 10 minutes. Protein detection was achieved using Western-Bright ECL Spray (Witec,

Switzerland) and visualized on Vilber Fusion FX system (Witec, Switzerland). The intensities of the signals were quantified using ImageJ software (NIH, USA), and the protein expression was normalized using α -tubulin (Sigma-Aldrich, USA) as a loading control.

Table 4: Antibodies used for Western Blot

	Antibody	Dilution	Host	Company
primary	PARP1	1:1,000	Mouse	BioRad
	TUJ1	1:2,000	Mouse	Sigma-Aldrich
	TH	1:1,000	Rabbit	Pel-Freez
	MAP2	1:1,000	Mouse	Sigma-Aldrich
	SYP	1:20,000	Rabbit	Abcam
	αSyn	1:500	Mouse	BioLegend
	S100β	1:1000	Rabbit	Abcam
	α-Tubulin	1:20,000	Mouse	Sigma-Aldrich
secondary	anti-mouse IgG HRP	1:5,000	Donkey	Thermo Fischer Scientific
	anti-rabbit IgG HRP	1:5,000	Donkey	Thermo Fischer Scientific

PARP1 = Poly (ADP-ribose) Polymerase 1, TUJ1 = β III-tubulin, TH = tyrosine hydroxylase, MAP2 = microtubule-associated protein 2, SYP = Synaptophysin, α Syn = α -synuclein, S100 β = S100 calciumbinding protein B, IgG = immunoglobulin G, HRP = horseradish peroxidase

Immunofluorescence

For immunofluorescence staining, cells were seeded at a density of 15'000 cells per well of a 96-well plate (Griener Bio-One, Germany), which were coated with PLO [15 µg/mL]-laminin [10 µg/mL] (Sigma-Aldrich, Germany). After differentiation and after maturation (Figure 2) cells were fixed with cold 4% paraformaldehyde (PFA; Sigma-Aldrich, Germany) for 10 minutes at RT. The blocking of the cells was done using 10% horse serum in PBS-0.8% Triton™ X100 (Sigma-Aldrich, Germany) for 2 hours at RT. After the blocking step, the cells were incubated with primary antibody (Table 5) diluted in 2.5% horse serum in PBS-0.4% Triton™ X100 overnight at 4°C. Four washing steps of 10 minutes in PBS were performed before the incubation with secondary antibodies. The secondary antibodies used are listed in table 5. Additionally, Hoechst 33342 (Life technologies, USA) was used as a nuclear staining. Incubation was performed for 2 hours at RT. After another four washing steps with PBS for 10 minutes each, images were acquired using the Cytation™ 10 Confocal Imaging Reader (Agilent BioTek, USA), and cell count analysis was subsequently conducted with Gen5™ software (Agilent BioTek, USA) to quantify labeled cells.

Table 5: Antibodies used for Immunofluorescence

	Antibody	Dilution	Host	Company
primary	TUJ1	1:500	Mouse	Sigma-Aldrich
	TH	1:1,000	Rabbit	Pel-Freez
	MAP2	1:500	Mouse	Sigma-Aldrich
	SYP	1:250	Rabbit	Abcam
secondary	anti-donkey AF IgG 647	1:250	Donkey	Thermo Fischer Scientific
	anti-rabbit AF IgG 488	1:250	Donkey	Thermo Fischer Scientific
other	Hoechst 33342	1:2,000		Life Technologies

TUJ1 = β -III-tubulin, TH = tyrosine hydroxylase, MAP2 = microtubule-associated protein 2, SYP = synaptophysin, AF = Alexa Fluor, IgG = immunoglobulin G

Statistical analysis

The differentiation of iPSCs into dopaminergic neurons was done four times, resulting in four independent runs. The IF analysis after differentiation included the assessment of β -III-tubulin (TUJ1) and tyrosine hydroxylase (TH) across all four runs, along with synaptophysin (SYP) and microtubule-associated protein 2 (MAP2) in two runs (Figure 2). The IF analysis after maturation involved the evaluation of all four markers - TUJ1, TH, SYP, and MAP2 - across three runs. For WB analysis, samples after differentiation and after maturation were assessed for TH, SYP, MAP2, and α -synuclein (α Syn) in four independent runs. Additionally, TUJ1 and PARP1 were analyzed in WB in three runs.

For the statistical analysis, eight conditions were defined based on WT or PARP1-KO, sham-exposed or RF-EMF-exposed and time point. Comparisons were conducted within and between these groups, specifically by comparing each cell condition at one time point with other conditions, both within the same time point and across time points. The data were examined using a one-way ANOVA, followed by Tukey's multiple comparison test. Analyses were conducted with GraphPad Prism software (GraphPad Software Inc., USA). Results are presented as the mean \pm standard error of the mean (SEM), and statistical significance was set at p \leq 0.05.

Results

Validation of the PARP1-KO

Sanger sequencing of the regions around the gRNA binding sites (gRNA1, gRNA2, gRNA3) showed a single nucleotide insertion at position 382 in the sequence targeted by gRNA2, relative to the hu-PARP1 control sequence. This insertion caused a frameshift, resulting in a shortened protein of 154 amino acids rather than the full-length of 1014 amino acids. Transfection using gRNA1 and gRNA3 did not lead to any mutation.



Figure 3: Sequence alignment of DNA-nucleotides of PARP1 wildtype (WT) and PARP knockout (KO) cells transfected with gRNA2. Arrow indicates insertion. Created with SnapGene software (https://www.snapgene.com)

Validation of pluripotency

Flow cytometry results showed that 89.6% of the double stained WT iPSCs were positive for both SSEA-5 and TRA-1-60 (Figure 4 B1-B5), while stained PARP1-KO iPSCs had an even higher double-positive rate of 99.7% (Figure 4 D1-D5). The unstained WT samples (Figure 4 A1-A5) confirmed minimal background fluorescence,

with 99.1% WT and 100% KO cells (Figure 6 C1-C5) were double-negative for both markers.

Cells were considered pluripotent for differentiation since more than 80% of the iPSCs were positive for both markers, SSEA-5 and TRA-1-60. Both WT and PARP1-KO cells met this criterion, confirming adequate stemness and suitability for further differentiation into dopaminergic neurons.

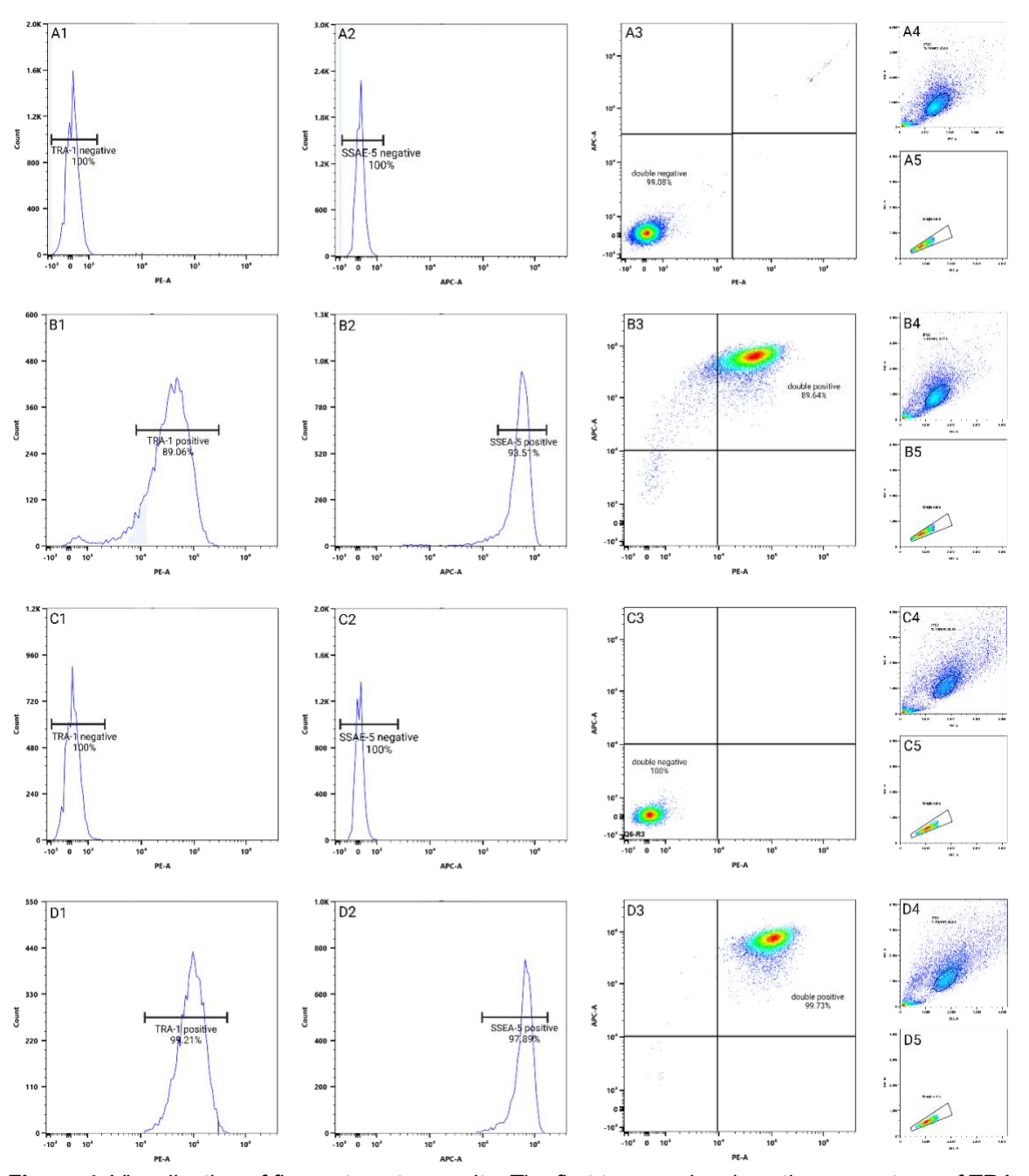


Figure 4: Visualization of flow cytometry results. The first two graphs show the percentage of TRA-1-60 positive/negative or SSEA-5-positive/negative cells in wild type (WT) iPSCs unstained (A1, A2), WT stained (B1, B2), knockout (KO) unstained (C1, C2), and KO stained (D1, D2). The third line shows the percentage of double positive cells of WT unstained (A3), WT stained (B3), KO unstained (C3) and KO stained (D3). A4, B4, C4 and D4 show the selected iPSC population from all events and the single cells from the iPSC population are shown in A5, B5, C5 and D5.

PARP1 protein levels

PARP1-KO iPSCs were generated to study the effect of PARP1 on neuronal differentiation and maturation. Additionally, the effect of RF-EMF was assessed in WT and PARP1-KO cells. PARP1 protein levels were analyzed at all conditions across both time points, namely after differentiation and after maturation.

A significant reduction of protein expression was observed in PARP1-KO cells, as confirmed by WB analysis, with protein levels significantly decreased after differentiation compared to WT cells, regardless of the RF-EMF exposure (Figure 5). Additionally, PARP1 levels were significantly reduced in WT cells after maturation when compared to WT cells after differentiation. PARP1-KO cells demonstrated very low if not absent PARP1 levels. No statistically significant differences in PARP1 levels were found in WT cells when RF-EMF exposure was compared to sham exposure regardless of the time during neuronal differentiation (Figure 5).

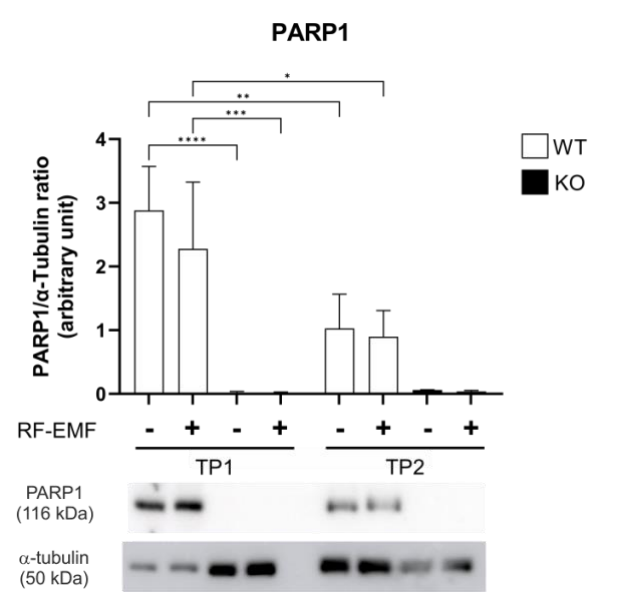


Figure 5: Protein levels of PARP1 in WT sham radiated (-) and radiated (+) and KO sham radiated (-) and radiated (+) from both time points (TP1 = after differentiation, TP2 = after 2 weeks maturation) from 3 independent experiments. The respective protein levels are given in arbitrary units after normalization on the expression of the housekeeping protein α -tubulin. Representative Western blots are shown under the graph. Significant differences are indicated by asterisks (* = p \leq 0.05, ** = p \leq 0.01, *** = p \leq 0.001, **** = p \leq 0.0001). Error bars represent SEM. RF-EMF = radio frequency electromagnetic field

Neuronal phenotype

TUJ1 and TH protein levels

To characterize the phenotype of young neurons, the neuron specific marker TUJ1 (Hausrat et al. 2021) was analyzed using WB and IF. TUJ1 levels revealed statistically significant differences (Figure 6A) with significantly higher levels in WT cells at the end of maturation compared to differentiation. The same trend was also observed in PARP1-KO cells even though there was only statistical significance in RF-EMF-exposed neurons. These findings suggest a consistent trend of increased TUJ1 expression and thus more neurons over time (Figure 6A). No significant differences were obtained between sham-exposed and RF-EMF-exposed cells, and WT and PARP1-KO cells, but a trend towards an increase in TUJ1 in irradiated PARP-1 KO cells compared to the respective sham-exposed cells was found after maturation (Figure 6A).

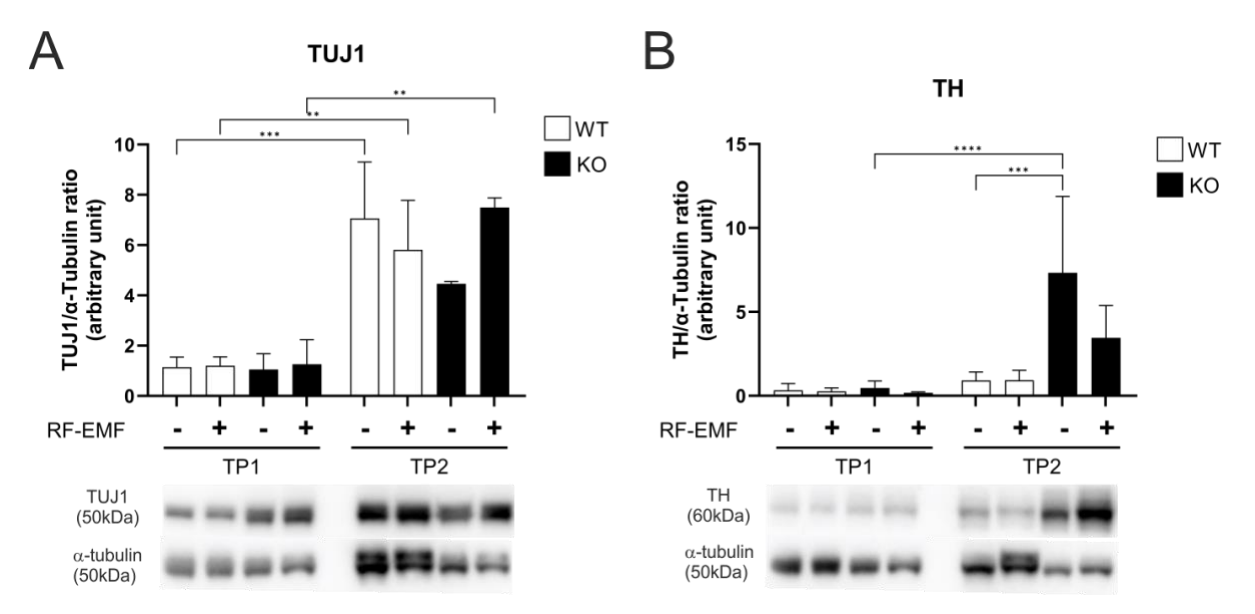


Figure 6: Protein levels of TUJ1 (A) and TH (B) in WT sham radiated (-) and radiated (+) and KO sham radiated (-) and radiated (+) from both time points (TP1 = after differentiation, TP2 = after 2 weeks maturation) from 3 independent experiments for TUJ1 and 4 independent experiments for TH. The respective protein levels are given in arbitrary units after normalization on the expression of the housekeeping protein α-tubulin. Representative Western blots are shown under the graph. Significant differences are indicated by asterisks (* = p ≤ 0.05, ** = p ≤ 0.01, *** = p ≤ 0.001, **** = p ≤ 0.0001). Error bars represent SEM. RF-EMF = radio frequency electromagnetic field.

TH, a key enzyme involved in dopamine synthesis, was used to identify dopaminergic neurons. WB analysis showed an increase in TH protein levels in PARP1-KO cells after maturation compared to differentiation, suggesting an increase of dopaminergic neurons (Figure 6B). In WT cells, no significant increase was observed in TH levels, but a trend was found towards an increase in TH levels during maturation. No statistical significance was observed between all sham-exposed cells compared to RF-EMF-exposed cells, but a decrease of TH expression in RF-EMF-exposed PARP1-KO cells was observed at the end of maturation (Figure 6B).

Similar to the findings in WB analyses, immunofluorescence analyses showed a significant increase in TUJ1 after maturation compared to WT cells after differentiation (Figure 7J). A visual increase of TUJ1 immunoreactive (-ir) cells can also be seen when comparing IF images of WT cells after differentiation to WT cells after maturation (Figure 7 A, D). RF-EMF-exposure did not result in statistically significant differences at both time points regardless of the cells being PARP1-KO or WT (Figure 7J).

An increase of TH-ir cells was observed in WT cells after maturation compared to differentiation, suggesting a higher expression as development progressed (Figure 7K). This time dependent increase in TH-ir cells was also observed in PARP1-KO cells after maturation, where it reached statistical significance for sham-exposed and RF-EMF-exposed cells. While a tendency for an increase in TH-ir cells was observed between WT and PARP1-KO cells after differentiation, this increase was significant after maturation. No differences were observed between sham and RF-EMF-radiated groups (Figure 7K).

Similar to the findings obtained in the WB analysis results, the IF data showed enhanced TH levels after maturation compared to differentiation (Figure 6B, 7K), with the effect only being statistically significant for PARP1-KO cells. No significant differences in TH levels were observed between RF-EMF-exposed cells and shamexposed cells at any time of development investigated.

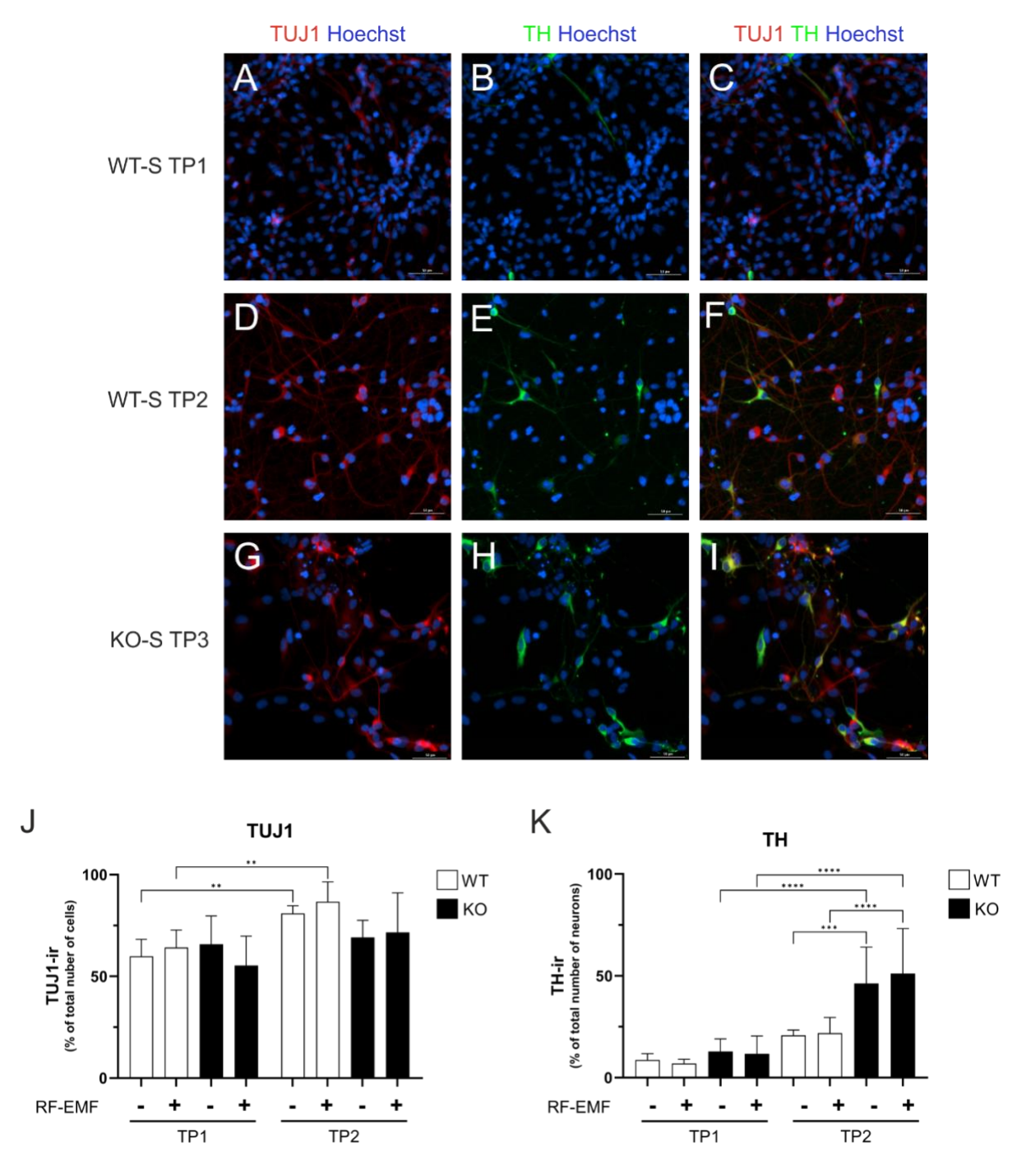


Figure 7: Representative immunofluorescence microscopy images of WT sham-radiated (WT-S) after differentiation (time point 1 (TP1)) (A-C) and after maturation (time point 2 (TP2)) (D-F) and KO sham radiated (KO-S) after maturation (time point 2 (TP2)) (G-H). Cells stained with TUJ1 (red) (A, D, G, C, F, I) and TH (green) (B, E, H, C, F, I). Cell nuclei were counterstained with Hoechst (blue). Magnification 20x, scale bars 50μm. Semi quantitative analyses of the number of TUJ1- (J) and TH-(K) immunoreactive (-ir) cells, indicating neuronal (J) and dopaminergic (K) phenotype in WT sham radiated (-) and radiated (+) and KO sham radiated (-) and radiated (+) from 4 independent experiments for time point 1 (TP1 = after differentiation) and 3 independent experiments for time point 2 (TP2 = after maturation). The data of TUJ1 represent the mean percentage of TUJ1-ir cells compared to the total number of cells (cell nuclei counterstained with Hoechst) and the data of TH represent the mean percentage of TH-ir cells compared to TUJ1-ir cells. Significant differences are indicated by asterisks (* = p ≤ 0.05, ** = p ≤ 0.01, *** = p ≤ 0.001, **** = p ≤ 0.0001). Error bars represent the SEM. RF-EMF = radio frequency electromagnetic field.

MAP2 protein levels

To identify mature neurons, MAP2, as a marker for neuronal differentiation and neurite outgrowth, was analyzed (Dehmelt and Halpain 2005). Two MAP2 isoforms, with a molecular weight of 70 kDa and 280 kDa, were analyzed by WB.

MAP2 expression increased in WT and PARP1-KO cells after maturation compared to differentiation, indicating a time-dependent increase in neuronal development (Figure 8). However, this increase was not statistically significant for both isoforms. Additionally, higher MAP2 levels were found in PARP1-KO cells after maturation when compared to WT cells. This increase was observed for both MAP2 isoforms, even though the increase was not statistically significant.

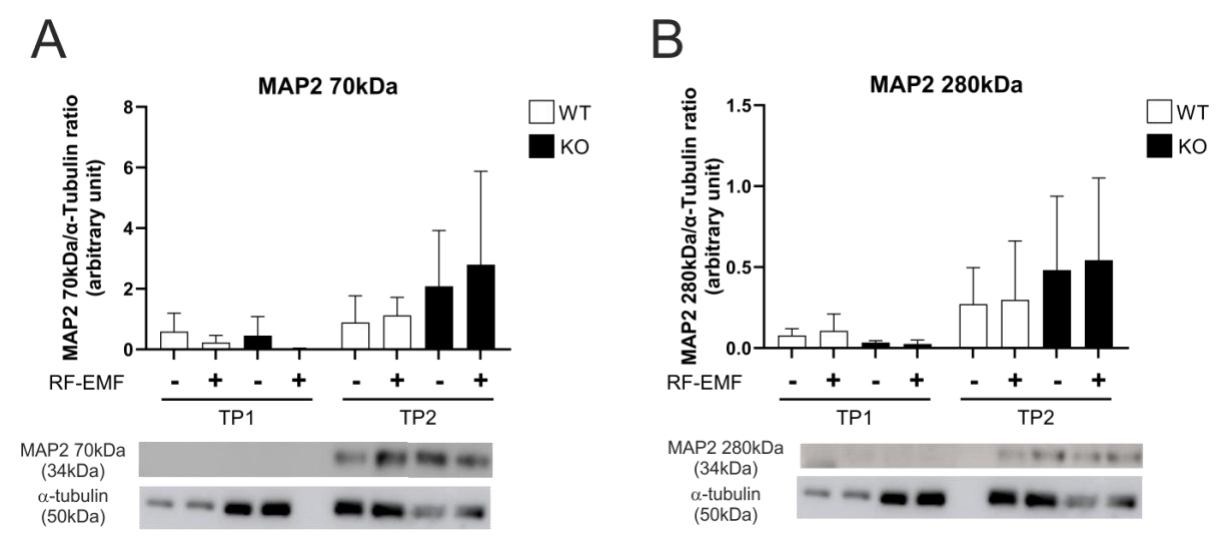


Figure 8: Protein levels of MAP2 70kDa (A) and MAP2 280kDa (B) in WT sham radiated (-) and radiated (+) and KO sham radiated (-) and radiated (+) from both time points (TP1 = after differentiation, TP2 = after 2 weeks maturation) from 4 independent experiments. The respective protein levels are given in arbitrary units after normalization on the expression of the housekeeping protein α-tubulin. Representative Western blots are shown under the graph. Significant differences are indicated by asterisks (* = p ≤ 0.05, ** = p ≤ 0.01, **** = p ≤ 0.001, **** = p ≤ 0.0001). Error bars represent the SEM. RF-EMF = radio frequency electromagnetic field.

MAP2 expression observed by IF analysis revealed significant increases after maturation compared to differentiation for both WT and PARP1-KO cells, indicating an overall increase in MAP2 expression over time (Figure 9 and Figure 10). No significant differences were detected between WT and PARP1-KO or between sham-exposed and RF-EMF-exposed within each time point. However, MAP2 levels in PARP1-KO cells were lower by trend compared to WT cells at differentiation (Figure 9). The increase in MAP2 over time was not altered by RF-EMF exposure compared to sham exposure.

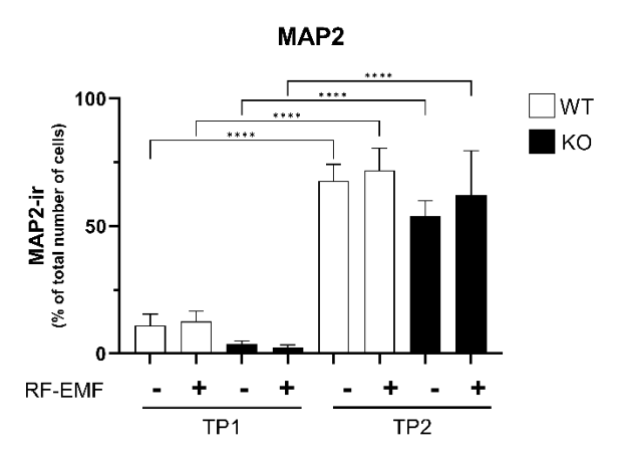


Figure 9: Semi quantitative analyses of the number of MAP2 immunoreactive (-ir) cells.in WT sham radiated (-) and radiated (+) and KO sham radiated (-) and radiated (+) from 2 independent experiments for time point 1 (TP1 = after differentiation) and 3 independent experiments for time point 2 (TP2 = after 2 weeks maturation). Data represent the mean percentage of immunoreactive cells compared to the total number of cells (cell nuclei counterstained with Hoechst). Significant differences are indicated by asterisks (* = p \leq 0.05, ** = p \leq 0.01, *** = p \leq 0.001, **** = p \leq 0.0001). Error bars represent the SEM. RF-EMF = radio frequency electromagnetic field.

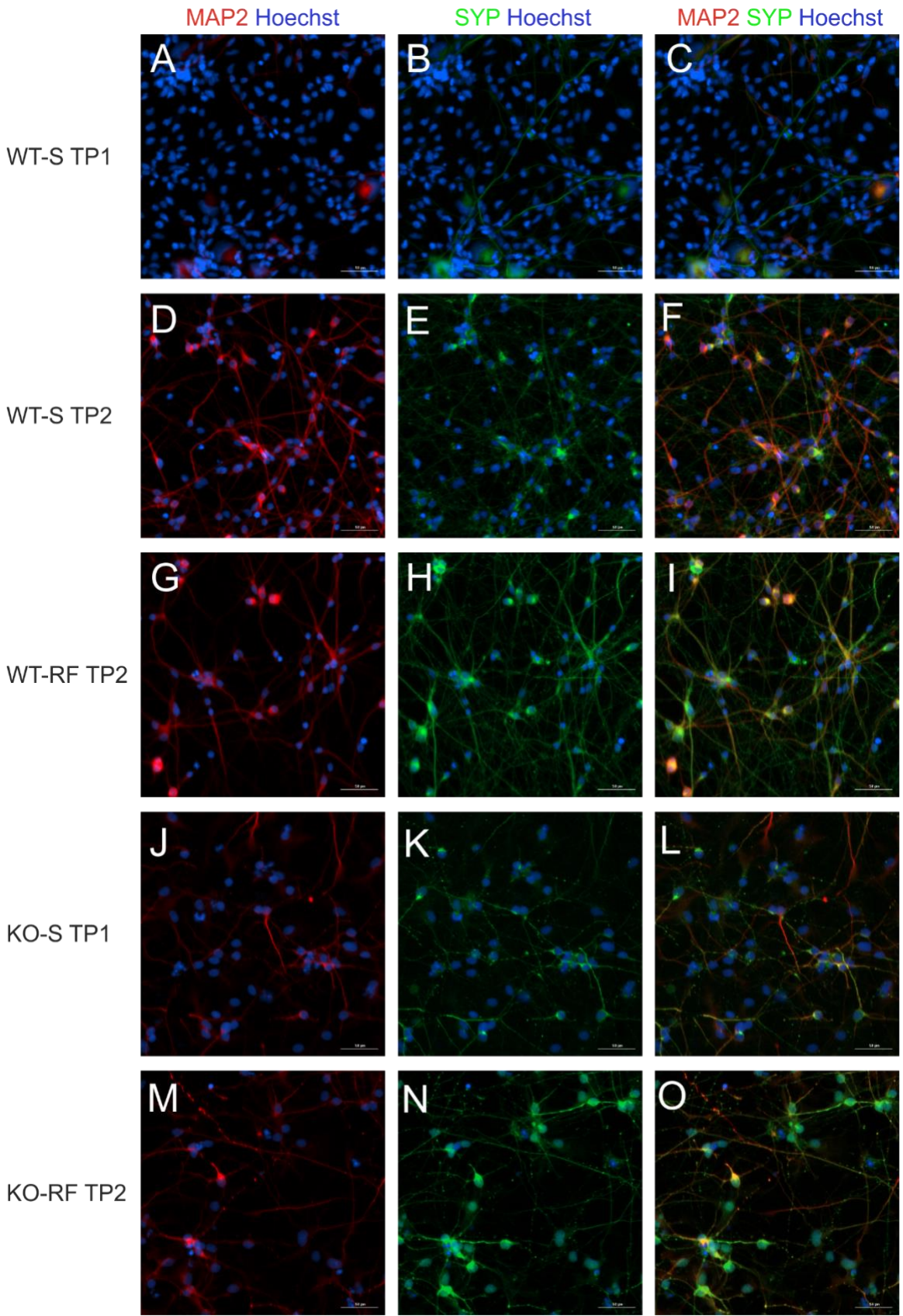


Figure 10: Representative immunofluorescence microscopy images of WT sham radiated (S) after differentiation (time point 1 (TP1)) (A-C) and after maturation (time point 2 (TP2)) (D-F), WT RF-EMF radiated (RF) after maturation (TP2), KO S TP2 (G-H) and KO-RF TP2. Cells stained with MAP2 (red) (A, D, G, C, F, I) and SYP (green) (B, E, H, C, F, I). Cell nuclei were counterstained with Hoechst (blue). Magnification 20x, scale bars 50μm

Synaptic plasticity

SYP protein levels

SYP, a presynaptic protein that marks synaptic vesicles and is essential for evaluating synapse formation (Calhoun et al. 1996). WB analysis showed an increase in SYP protein levels in WT cells after maturation compared to differentiation (Figure 11) but the only PARP1-KO cells reached statistical significance. These findings suggest a time-dependent increase in SYP protein levels. In addition, the increase in SYP protein levels was more pronounced for PARP1-KO cells after maturation compared to the WT cells, although this increase was not statistically significant. No significant differences were observed between the sham-exposed and RF-EMF-exposed cells for PARP1-KO as well as WT (Figure 11).

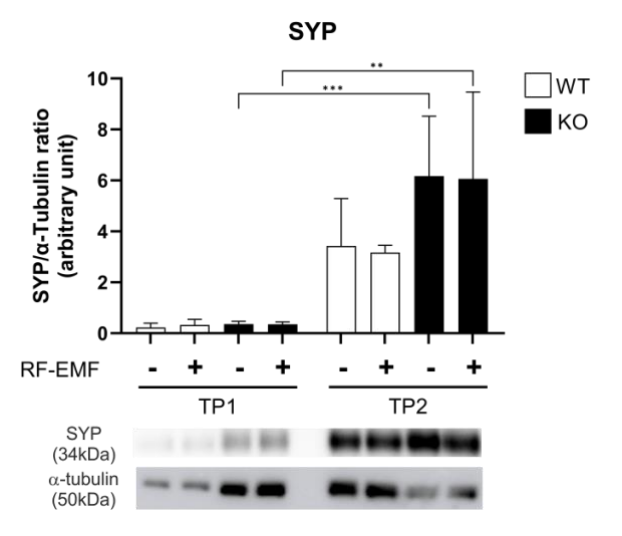


Figure 11: Protein levels of SYP in WT sham radiated (-) and radiated (+) and KO sham radiated (-) and radiated (+) from both time points (TP1 = after differentiation, TP2 = after 2 weeks maturation) from 4 independent experiments. The respective protein levels are given in arbitrary units after normalization on the expression of the housekeeping protein α-tubulin. Representative Western blots are shown under the graph. Significant differences are indicated by asterisks (* = p ≤ 0.05, ** = p ≤ 0.01, *** = p ≤ 0.001, *** = p ≤ 0.0001). Error bars represent SEM. RF-EMF = radio frequency electromagnetic field.

Immunofluorescence analysis of SYP revealed significant increases in the number of SYP-ir cells in WT as well as in PARP1-KO cells after maturation compared to differentiation (Figures 10 and 12). Additionally, after maturation, the number of SYP-ir cells was significantly higher in RF-EMF-exposed cells compared to sham-exposed cells in both WT and PARP1-KO cells. These results suggest an upregulation of SYP expression under RF-EMF exposure.

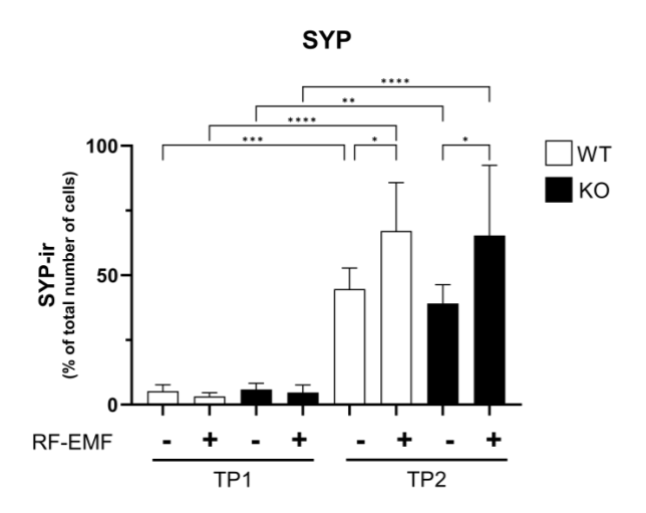


Figure 12: Semi quantitative analyses of the number of SYP immunoreactive (-ir) cells.in WT sham radiated (-) and radiated (+) and KO sham radiated (-) and radiated (+) from 2 independent experiments for time point 1 (TP1 = after differentiation) and 3 independent experiments for time point 2 (TP2 = after 2 weeks maturation). Data represent the mean percentage of immunoreactive cells compared to the total number of cells (cell nuclei counterstained with Hoechst). Significant differences are indicated by asterisks (* = p \leq 0.05, ** = p \leq 0.01, *** = p \leq 0.001, **** = p \leq 0.0001). Error bars represent SEM, RF-EMF = radio frequency electromagnetic field

αSyn protein levels

 α Syn has been prominently associated with synaptic function and its impact in neurodegenerative diseases such as PD has been described (Morris et al. 2024). WB analysis of α Syn showed an increase in protein levels in WT cells after maturation compared to differentiation, although the effect was only statistically significant in RF-EMF-exposed cells (Figure 13). α Syn levels were also more pronounced in PARP1-KO cells after maturation compared to differentiation. However, this effect was not statistically significant. Additionally, after maturation, α Syn levels were lower in PARP1-KO cells by trend when compared to WT cells.

The results suggest an increase in α Syn protein levels over time with the effect being less pronounced in PARP1-KO cells compared to WT cells.

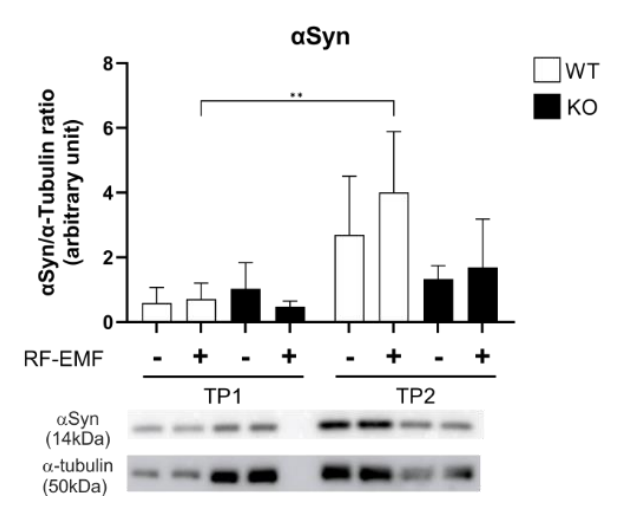


Figure 13: Protein levels of αSyn in WT sham radiated (-) and radiated (+) and KO sham radiated (-) and radiated (+) from both time points (TP1 = after differentiation, TP2 = after 2 weeks maturation) from 4 independent experiments. The respective protein levels are given in arbitrary units after normalization on the expression of the housekeeping protein α-tubulin. Representative Western blots are shown under the graph. Significant differences are indicated by asterisks (* = p \leq 0.05, ** = p \leq 0.001, *** = p \leq 0.001, *** = p \leq 0.0001). Error bars represent SEM, RF-EMF = radio frequency electromagnetic field.

Glial marker

S100β protein levels

S100 β , a marker for astrocytes in the central nervous system (CNS) (Michetti et al. 2023) was analyzed in the exposure conditions described before. A significant increase in S100 β protein levels was observed in WT sham-exposed cells after maturation compared to WT sham exposed cells after differentiation (Figure 14). The same trend was seen in WT RF-EMF-exposed cells, but this increase did not reach statistical significance. Higher S100 β protein levels were also found in PARP1-KO cells after maturation compared to differentiation by trend. These findings suggest an overall trend toward increased S100 β expression over time.

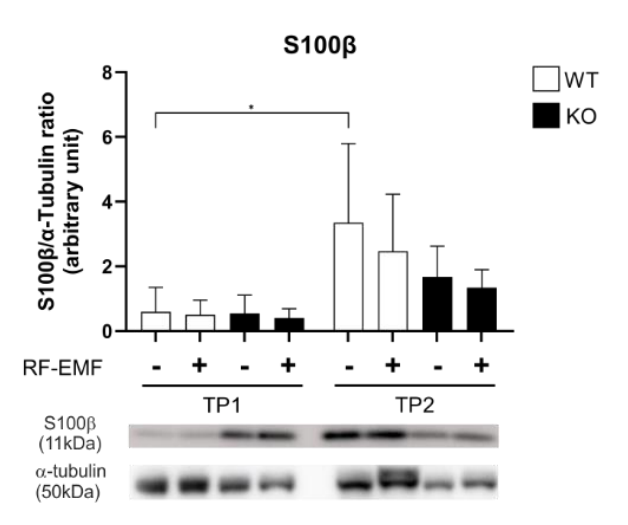


Figure 14: Protein levels of S100β in WT sham radiated (-) and radiated (+) and KO sham radiated (-) and radiated (+) from both time points (TP1 = after differentiation, TP2 = after 2 weeks maturation) from 4 independent experiments. The respective protein levels are given in arbitrary units after normalization on the expression of the housekeeping protein α-tubulin. Representative Western blots are shown under the graph. Significant differences are indicated by asterisks (* = p \leq 0.05, ** = p \leq 0.01, *** = p \leq 0.001, *** = p \leq 0.0001). Error bars represent SEM. RF-EMF = radio frequency electromagnetic field.

Discussion

Results from this study provide new insights into the role of PARP1 in neuronal development, particularly during differentiation and maturation, and effects of 5G NR FR1 in WT and PARP1-KO cells. PARP1-KO, generated using CRISPR/Cas9, yielded a successful frameshift mutation, confirmed by Sanger sequencing. This frameshift resulted in significantly reduced PARP1 protein levels compared to WT cells.

PARP1 protein level was notably lower in WT cells after maturation compared to differentiation. This aligns with a previously published study, suggesting that PARP1 activity is modulated according to cellular developmental stages (W. Chen et al. 2022). PARP1's role in neural progenitor cell differentiation, suggests that its regulation may be dynamically linked to specific developmental stages (W. Chen et al. 2022). This gradual decrease could signify PARP1's shift from involvement in DNA repair to more specialized neuronal functions, aligning with data demonstrating PARP1's essential role in myelination during CNS development (Wang et al. 2021).

Our data did not reflect any significant changes in PARP1 levels following RF-EMF exposure. The exposure was conducted during the induction phase, and therefore, we cannot exclude that RF-EMF exposure at a different stage, such as during differentiation or maturation, affects PARP1 levels. Our findings are in contrast with results by He et al. (2017), who observed that RF-EMF exposure (900 MHz, SAR of 120 µW/cm²) for 3 hours/day for 5 days induced PARP1 activation, suggesting that RF-EMF may initiate cellular stress responses involving PARP1 in certain conditions. Differences in the findings might be caused by variations in the experimental design, RF-EMF exposure parameters, or cell types used, highlighting the complexity of RF-EMF effects on cellular function and involved players, and the need for further investigations to evaluate the role of PARP1 in RF-EMF-induced cellular responses.

To assess differentiation and maturation in the development of dopaminergic neurons, we investigated TUJ1 as a marker for younger neurons and MAP2 for more mature neurons. We observed a significant increase in TUJ1 expression in WT cells at the end of maturation compared to differentiation regardless of the analysis methods used, indicating a time-dependent rise in neuronal populations. A similar trend was found in PARP1-KO cells, although statistical significance was only reached in WB in RF-EMF-exposed cells. We found no difference in RF-EMF-exposed cells compared to sham-

exposed cells which contrasts with other studies showing that RF-EMF can affect neuronal differentiation and cell proliferation (C. Chen et al. 2021; Eghlidospour et al. 2017). An effect in RF-EMF exposure at 900 MHz (SAR of 2.3 W/kg) has been shown to affect neural stem cell proliferation and differentiation in mice, suggesting its impact on early neuronal development (Eghlidospour et al. 2017). Similarly, inhibited neurite outgrowth was demonstrated in neural cells after RF-EMF exposure at 1800 MHz, likely by disrupting Eph receptors 5 (EPHA5) signaling, which is required for neurite outgrowth (C. Chen et al. 2021). It is important to note, however, that the cell types and experimental models used in these referenced studies differ significantly from ours. While we used human iPSCs in our study, they used neural stem cells derived from mice (Eghlidospour et al. 2017), or Neuro-2A cells (C. Chen et al. 2021). Frequencies and SAR levels also differed significantly from those used in the present study. All these differences limit direct comparability with our findings, highlighting the need for further research to clarify the influence of RF-EMF exposure on human neuronal differentiation.

Investigations on the maturity of the developed dopaminergic neurons were studied with and without RF-EMF exposure. As expected, an upregulation of MAP2 was observed after maturation compared to differentiation, suggesting a time dependent increase of mature neurons. MAP2 levels were reported to correlate with neuronal maturation (Dehmelt and Halpain 2005). Similar findings were also obtained in PARP1-KO cells after maturation compared to WT cells. This more subtle increase in PARP1-KO cells may suggest that the PARP1-KO influences neuronal maturation but due to the lack of significance, further experiments are needed to evaluate the influence of PARP1 on neuronal maturation. No significant differences in MAP2 expression were found when RF-EMF-exposed and sham-exposed cells were compared. In contrast to these findings, alterations of MAP2 protein levels after RF-EMF exposure have been reported (Kim et al. 2021; R. Zhao et al. 2007). RF-EMF exposure at 1760 MHz at a SAR of 4.0 W/kg for 5 hours per day over 9 days was found to hinder neurite outgrowth and alter postsynaptic structures in hippocampal neurons in mice, leading to a decrease in MAP2 expression (Kim et al. 2021). In contrast, an upregulation in MAP2 levels was found in rat neurons exposed to RF-EMF for 24 hours (1800 MHz, SAR 2 W/kg) (R. Zhao et al. 2007). Again, differences in experimental models, including species, cell types, and RF-EMF exposure parameters, might explain the differences

in findings across studies, suggesting that further research is necessary to understand the influence of RF-EMF on neuronal maturation.

Analyses of the dopaminergic phenotype were investigated using the marker TH, a rate-limiting enzyme in dopamine synthesis, reflects dopaminergic neuron health and function (Harsing 2008). A significant increase of dopaminergic neurons was obtained following maturation in both WT and PARP1-KO cells, with statistical significance achieved only in PARP1-KO cells. This time-dependent upregulation of dopaminergic neurons in PARP1-KO cells indicates that the absence of PARP1 may promote neuronal differentiation and maturation into dopaminergic neurons, and a possible role of PARP1 in regulating cellular signaling linked to dopaminergic function. These regarding the phenotype may have important implications findings neurodegenerative diseases such as PD, where the loss of dopaminergic neurons is a hallmark (Lengyel-Zhand et al. 2022). The observed promotion of dopaminergic neurons in absence of PARP1 suggests that it may act as a negative regulator in the development or maintenance of these neurons. Targeting PARP1 or its associated pathways could, therefore, represent a novel therapeutic strategy to support regeneration of dopaminergic neurons or diminished development and/or progression of neurodegeneration. The neuroprotective effect of PARP1 inhibition was demonstrated by Lu et al. (2017). They showed that nicotine treatment reduced PARP1 activity and preserved TH expression in PD models, mitigating the loss of TH-positive neurons in 6-OHDA-lesioned mice and ETC complex I inhibitor methylpyridinium ion (MPP+) treated neuron-like SH-SY5Y cells (Lu et al. 2017). A comparison between the study by Lu et al. (2017) and ours is challenging, PARP1 was knocked out using genetic engineering methods in our research, whereas Lu et al. (2017) suppressed PARP1 using biochemical methods. Furthermore, the study models differ in terms of the cell types used. Further research is necessary to explore how modulating PARP1 activity affects the survival of dopaminergic neurons and function in disease models, potentially providing new insights into treatments for PD and related disorders. Interestingly, while we did not obtain statistically significant differences between shamexposed and RF-EMF-exposed cells, a trend toward a decrease of dopaminergic neurons was observed in RF-EMF-exposed PARP1-KO cells at the end of maturation. Although this reduction was not statistically significant, it points towards a potential influence of RF-EMF exposure on the development of dopaminergic neurons in PARP1-KO. This observation supports findings from previously published studies.

reporting that RF-EMF exposure impairs dopaminergic function and dopamine regulation (Kim et al. 2019). Reduced dopamine levels and fewer dopaminergic striatal neurons in C57BL/6 mice were demonstrated after RF-EMF exposure at 835 MHz for 5 h/day for 12 weeks (SAR of 4.0 W/kg). Similarly, changes in dopamine levels across various brain regions were demonstrated in rats following RF-EMF exposure (1800 MHz, SAR of 0.843 W/kg) (Aboul Ezz et al. 2013), further supporting effects of RF-EMF on dopaminergic neurotransmission. However, differences in the experimental settings and the use of *in vivo* models with long-term RF-EMF exposure might lead to different outcomes. We used an *in vitro* system with human iPSC-derived dopaminergic neurons exposed for 33 hours during the induction phase towards the development of dopaminergic neurons. These differences limit direct comparability but underscore the need for further research of RF-EMF exposure and possible effects on neurodegeneration using disease models.

To assess synaptic function, SYP and αSyn were analyzed, two proteins critical for neuronal function and associated with neurodegenerative diseases (Bai and Strong 2014). SYP, a presynaptic vesicle protein, is widely recognized as a marker of synapse formation, providing valuable insights into synaptic density and function (Bai and Strong 2014). Our findings showed a time-dependent increase in SYP expression, indicating enhanced synaptic formation as neuronal development progresses. This increase was demonstrated in both WT and PARP1-KO cells. The elevated SYP levels after maturation for RF-EMF-exposed cells compared to sham-exposed cells suggests that RF-EMF exposure may enhance synaptic formation, and it aligns with the hypothesis that RF-EMF exposure can modulate neuronal properties but contrasts with findings from a study showing detrimental impacts on neural systems (El Khoueiry et al. 2018). The impact of RF-EMF exposure (1800 MHz) on neuronal activity was investigated using multi-electrode arrays with neuronal cultures derived from rat embryonic cortices (El Khoueiry et al. 2018). In their study, a significant reduction was observed in spontaneous burst activity during 15 minutes of RF-EMF exposure at SAR values ranging from 0.01 to 9.2 W/kg. This reduction became more pronounced with increasing SAR levels and persisted at the highest SAR values, indicating a potential inhibitory effect of RF-EMF on neuronal activity (El Khoueiry et al. 2018). Similarly, it was observed that exposure to an 835 MHz RF-EMF at a SAR of 4.0 W/kg resulted in significant changes in the synaptic structure of cortical neurons. (Kim et al. 2017). A decrease in the density of synaptic vesicles in presynaptic boutons was noted.

accompanied by a reduction in the gene and protein expression levels of synapsin I/II, which are critical for neurotransmitter release (Kim et al. 2017). Additionally, a significant decrease in SYP levels was observed in midbrain organoids after 48 hours of RF-EMF exposure with an ON/OFF cycle of 7 minutes on and 40 minutes off (1950 MHz, SAR of 0.5 W/kg), further emphasizing potential adverse effects of RF-EMF exposure on synaptic integrity in specific contexts (Thomas et al. 2023).

We also investigated synaptic function using αSyn, a protein that plays a critical role in synaptic function and is strongly implicated in neurodegenerative diseases like PD (Dehay et al. 2015; Kalia and Kalia 2015). Our results showed a time-dependent increase in αSyn levels in WT cells post-maturation. This finding aligns with previous research demonstrating that RF-EMF (1800 MHz, SAR of 0.23 W/kg) exposure for three 10-minute sessions affects asyn metabolism in human neuroblastoma cells (Stefi et al. 2019). In our study, αSyn levels also increased post maturation in PARP1-KO cells but were lower compared to WT cells. This reduction in αSyn expression in PARP1-KO cells may indicate a protective effect in the absence of PARP1, as lower αSyn levels could mitigate its aggregation and associated neurotoxicity (Garcia-Reitboeck et al. 2013; Koch et al. 2015). Selective knockdown of αSyn in monoamine neurons via intranasal delivery of oligonucleotides reduced its levels in the substantia nigra and other key brain regions without causing neurodegeneration (Alarcón-Arís et al. 2018). This reduction enhanced dopamine and serotonin release, and the authors highlighting its potential as a therapeutic target for PD (Alarcón-Arís et al. 2018). Our results suggest that the depletion of PARP1 may inhibit αSyn, potentially providing a therapeutic approach for PD. The lack of significance in our study and the differing study models between ours and the referenced studies indicate that further research is essential to determine the relationship between PARP1 and αSyn and whether it could serve as a viable therapeutic target.

Astrocytes play crucial roles in maintaining neuronal health, supporting synaptic function, and modulating neuroinflammation, which is increasingly recognized as a contributing factor in neurodegenerative diseases (Li et al. 2019). Analyzing S100β expression can therefore offer insights into potential glial activation and astrocytic responses under PARP1-KO and RF-EMF conditions. Our analysis demonstrated a time dependent increase in astrocytes, similar to another study showing that astrocyte levels increase during neural development (Farhy-Tselnicker and Allen 2018).

Interestingly, both WT and PARP1-KO cells exposed to RF-EMF showed a trend toward fewer astrocytes after maturation compared to sham-exposed cells, though this difference was not statistically significant. This may imply a subtle RF-EMF influence on astrocytic activity, aligning with studies showing glial changes in response to RF-EMF exposure (Ammari et al. 2008; Barthélémy et al. 2016). These findings are also consistent with observations reporting a significant decrease in S100β levels in RF-EMF-exposed (1950 MHz, SAR of 0.5 W/kg) midbrain organoids compared to sham-exposed organoids at day 30 of development, though no differences were observed at day 60 (Thomas et al. 2023). Although the same cell model was used, comparing the two studies is challenging due to differences in radiation parameters. Nevertheless, the findings suggest that RF-EMF may impact astrocytes irrespective of the experimental conditions.

Conclusion

In this study, PARP1-KO cells were successfully generated from human iPSCs and differentiated into dopaminergic neurons. We have demonstrated that depletion of PARP1 may positively influence the development of dopaminergic neurons. Additionally, there are some indications for PARP1 playing a role in synaptic functions. RF-EMF exposure at 1950 MHz at a SAR of 4 W/kg for 33 hours during the induction phase did not alter the development of dopaminergic neurons nor the maturation of neurons.

These findings offer important insights into potential effects of RF-EMF radiation, the role of PARP1 in neuronal development, and its therapeutic prospects for neurodegenerative diseases. Future research focusses on investigations of RF-EMF exposure at different developmental stages to examine the role of PARP1 further. Additionally, integrating disease models will be used to provide insights into the therapeutic potential of targeting PARP1 in neurodegeneration. These approaches will advance understanding of neuronal development and therapeutic strategies.

References

- Aboul Ezz, H.S., Y.A. Khadrawy, N.A. Ahmed, N.M. Radwan, and M.M. El Bakry. 2013. "The Effect of Pulsed Electromagnetic Radiation from Mobile Phone on the Levels of Monoamine Neurotransmitters in Four Different Areas of Rat Brain." Eur Rev Med Pharmacol Sci 17-N. 13: 1782–88.
- Alarcón-Arís, D., A. Recasens, M. Galofré, I. Carballo-Carbajal, N. Zacchi, E. Ruiz-Bronchal, R. Pavia-Collado, et al. 2018. "Selective α-Synuclein Knockdown in Monoamine Neurons by Intranasal Oligonucleotide Delivery: Potential Therapy for Parkinson's Disease." *Molecular Therapy* 26(2): 550–67.
- Ammari, M., E. Brillaud, C. Gamez, A. Lecomte, M. Sakly, H. Abdelmelek, and R. de Seze. 2008. "Effect of a Chronic GSM 900 MHz Exposure on Glia in the Rat Brain." *Biomedicine & Pharmacotherapy* 62(4): 273–81.
- Arruri, V. K., C. Gundu, I. Khan, D. K. Khatri, and S. B. Singh. 2021. "PARP Overactivation in Neurological Disorders." *Mol Biol Rep* 48(3): 2833–41.
- Aslan, N. S., G. Orhan, and B. Karahalil. 2020. "The Impacts of Prominent Gene Polymorphisms in DNA Repair Enzymes on Parkinson's Disease." *Neuroscience Letters* 735.
- Azarm, K., and S. Smith. 2020. "Nuclear PARPs and Genome Integrity." *Genes and Development* 34(5): 285–301.
- Bai, X., and R. Strong. 2014. "Expression of Synaptophysin Protein in Different Dopaminergic Cell Lines." *Journal of biochemical and pharmacological research* 2(4): 185.
- Bandara, P., and S. Weller. 2018. Biological Effects of Low-Intensity Radiofrequency Electromagnetic Radiation-Time for a Paradigm Shift in Regulation of Public Exposure.

 https://www.researchgate.net/publication/325176291 Biological Effects of Low-intensity Radiofrequency Electromagnetic Radiation
 Time for a Paradigm Shift in Regulation of Public Exposure#full-text
- Barthélémy, A., A. Mouchard, M. Bouji, K. Blazy, R. Puigsegur, and A. S. Villégier. 2016. "Glial Markers and Emotional Memory in Rats Following Acute Cerebral Radiofrequency Exposures." Environmental Science and Pollution Research 23(24): 25343–55.
- Calhoun, M. E., M. Jucker, L. J. Martin, G. Thinakaran, D. L. Price, and P. R. Mouton. 1996. "Comparative Evaluation of Synaptophysin-Based Methods for Quantification of Synapses." *Journal of Neurocytology* 25(1): 821–28.
- Chen, C., Q. Ma, P. Deng, M. Lin, P. Gao, M. He, Y. Lu, et al. 2021. "1800 MHz Radiofrequency Electromagnetic Field Impairs Neurite Outgrowth Through Inhibiting EPHA5 Signaling." Frontiers in Cell and Developmental Biology 9: 657623.
- Chen, W, X. Chen, X. Zhang, C. Chen, S. Dan, J. Hu, B. Kang, and Y. J. Wang. 2022. "DNA Repair Proteins Cooperate with SOX2 in Regulating the Transition of Human Embryonic Stem Cells to Neural Progenitor Cells." *Biochem Biophys Res Commun* 586: 163–70.
- Dehay, B., M. Bourdenx, P. Gorry, S. Przedborski, M. Vila, S. Hunot, A. Singleton, et al. 2015. "Targeting α -Synuclein for Treating Parkinson's Disease: Mechanistic and Therapeutic Considerations." *The Lancet. Neurology* 14(8): 855.
- Dehmelt, L., and S. Halpain. 2005. "The MAP2/Tau Family of Microtubule-Associated Proteins." Genome Biology 6(1): 1–10.
- Eghlidospour, M., A. Ghanbari, S. M. J. Mortazavi, and H. Azari. 2017. "Effects of Radiofrequency Exposure Emitted from a GSM Mobile Phone on Proliferation, Differentiation, and Apoptosis of Neural Stem Cells." *Anatomy & Cell Biology* 50(2): 115.
- Farhy-Tselnicker, I., and N. J. Allen. 2018. "Astrocytes, Neurons, Synapses: A Tripartite View on Cortical Circuit Development." *Neural Development* 13(1).
- FOEN. 2024. "BERENIS Swiss Expert Group on Electromagnetic Fields and Non-Ionising Radiation.", Accessed 19.11.2024
 - https://www.bafu.admin.ch/bafu/en/home/topics/electrosmog/newsletter-of-the-swiss-expert-group-on-electromagnetic-fields-a/beratende-expertengruppe-nis-berenis.html

- Garcia-Reitboeck, P., O. Anichtchik, J. W. Dalley, N. Ninkina, G. K. Tofaris, V. L. Buchman, and M. G. Spillantini. 2013. "Endogenous Alpha-Synuclein Influences the Number of Dopaminergic Neurons in Mouse Substantia Nigra." *Experimental Neurology* 248: 541–45.
- Harsing, L. G. 2008. "Dopamine and the Dopaminergic Systems of the Brain." In *Handbook of Neurochemistry and Molecular Neurobiology*, ed. A. Lajtha. Boston: Springer: 149-170.
- Hausrat, T. J., J. Radwitz, F. L. Lombino, P. Breiden, and M. Kneussel. 2021. "Alpha- and Beta-Tubulin Isotypes Are Differentially Expressed during Brain Development." *Developmental Neurobiology* 81(3): 333–50.
- He, Q. N., L. Zong, Y. L. Sun, T. J. Prihoda, J. Tong, and Y. Cao. 2017. "Adaptive Response in Mouse Bone Marrow Stromal Cells Exposed to 900 MHz Radiofrequency Fields: Impact of Poly (ADP-Ribose) Polymerase (PARP)." Mutation Research-Genetic Toxicology and Environmental Mutagenesis 820: 19–25.
- Houldsworth, A. 2024. "Role of Oxidative Stress in Neurodegenerative Disorders: A Review of Reactive Oxygen Species and Prevention by Antioxidants." *Brain Communications* 6(1).
- Hu, M. L., Y. R. Pan, Y. Y. Yong, Y. Liu, L. Yu, D. L. Qin, G. Qiao, et al. 2023. "Poly (ADP-Ribose) Polymerase 1 and Neurodegenerative Diseases: Past, Present, and Future." *Ageing Research Reviews* 91: 102078.
- Huang, P., G. Chen, W. Jin, K. Mao, H. Wan, and Y. He. 2022. "Molecular Mechanisms of Parthanatos and Its Role in Diverse Diseases." *International Journal of Molecular Sciences* 23(13): 7292.
- IBM. 2024. "What Is 5G?", Accessed 07.11.2024. https://www.ibm.com/topics/5g
- Kalia, L. V., and S. K. Kalia. 2015. "α-Synuclein and Lewy Pathology in Parkinson's Disease." *Current Opinion in Neurology* 28(4): 375–81.
- Kaur, P., U. Rai, and R. Singh. 2023. "Genotoxic Risks to Male Reproductive Health from Radiofrequency Radiation." *Cells* 12(4): 594.
- El Khoueiry, C., D. Moretti, R. Renom, F. Camera, R. Orlacchio, A. Garenne, F. Poulletier De Gannes, et al. 2018. "Decreased Spontaneous Electrical Activity in Neuronal Networks Exposed to Radiofrequency 1,800 Mhz Signals." *Journal of Neurophysiology* 120(6): 2719–29.
- Kim, J. H., K. H. Chung, Y. R. Hwang, H. R. Park, H. J. Kim, H. G. Kim, and H. R. Kim. 2021. "Exposure to Rf-Emf Alters Postsynaptic Structure and Hinders Neurite Outgrowth in Developing Hippocampal Neurons of Early Postnatal Mice." *International Journal of Molecular Sciences* 22(10): 5340.
- Kim, J. H., H. J. Kim, D. H. Yu, H. S. Kweon, Y. H. Huh, and H. R. Kim. 2017. "Changes in Numbers and Size of Synaptic Vesicles of Cortical Neurons Induced by Exposure to 835 MHz Radiofrequency-Electromagnetic Field." *PLOS ONE* 12(10): e0186416.
- Kim, J. H., C. H. Lee, H. G. Kim, and H. R. Kim. 2019. "Decreased Dopamine in Striatum and Difficult Locomotor Recovery from MPTP Insult after Exposure to Radiofrequency Electromagnetic Fields." *Scientific Reports 2019 9:1* 9(1): 1–13.
- Knott, A. B., G. Perkins, R. Schwarzenbacher, and E. Bossy-Wetzel. 2008. "Mitochondrial Fragmentation in Neurodegeneration." *Nature Reviews Neuroscience* 9(7): 505–18.
- Koch, J. C., F. Bitow, J. Haack, Z. Hedouville, J. N. Zhang, L. Tönges, U. Michel, et al. 2015. "Alpha-Synuclein Affects Neurite Morphology, Autophagy, Vesicle Transport and Axonal Degeneration in CNS Neurons." *Cell Death & Disease 2015 6:7* 6(7): e1811–e1811.
- Korovesis, D., T. Rubio-Tomás, and N. Tavernarakis. 2023. "Oxidative Stress in Age-Related Neurodegenerative Diseases: An Overview of Recent Tools and Findings." *Antioxidants* 12(1): 131.
- Krishnakumar, R., and W. L. Kraus. 2010. "The PARP Side of the Nucleus: Molecular Actions, Physiological Outcomes, and Clinical Targets." *Molecular Cell* 39(1): 8–24.
- Kumari, K., H. Koivisto, M. Viluksela, K. M. A. Paldanius, M. Marttinen, M. Hiltunen, J. Naarala, H. Tanila, and J. Juutilainen. 2017. "Behavioral Testing of Mice Exposed to Intermediate Frequency Magnetic Fields Indicates Mild Memory Impairment." *PLoS ONE* 12(12): e0188880.
- Labun, K., T. G. Montague, M. Krause, Y. N. Torres Cleuren, H. Tjeldnes, and E. Valen. 2019. "CHOPCHOP v3: Expanding the CRISPR Web Toolbox beyond Genome Editing." *Nucleic Acids Research* 47(W1): W171–74.

- Lengyel-Zhand, Z, L. N. Puentes, and R. H. Mach. 2022. "PARkinson's: From Cellular Mechanisms to Potential Therapeutics." *Pharmacol Ther* 230: 107968.
- Li, K., J. Li, J. Zheng, and S. Qin. 2019. "Reactive Astrocytes in Neurodegenerative Diseases." *Aging and Disease* 10(3): 664.
- Liu, L., J. Li, Y. Ke, X. Zeng, J. Gao, X. Ba, and R. Wang. 2022. "The Key Players of Parthanatos: Opportunities for Targeting Multiple Levels in the Therapy of Parthanatos-Based Pathogenesis." *Cellular and Molecular Life Sciences* 79(1): 60.
- Lu, J. Y. D., P. Su, J. E. M. Barber, J. E. Nash, A. D. Le, F. Liu, and A. H. C. Wong. 2017. "The Neuroprotective Effect of Nicotine in Parkinson's Disease Models Is Associated with Inhibiting PARP-1 and Caspase-3 Cleavage." *PeerJ* 2017(10): e3933.
- Mao, K., and G. Zhang. 2022. "The Role of PARP1 in Neurodegenerative Diseases and Aging." *FEBS J* 289(8): 2013–24.
- Michetti, F., M. E. Clementi, R. Di Liddo, F. Valeriani, F. Ria, M. Rende, G. Di Sante, and V. R. Spica. 2023. "The S100B Protein: A Multifaceted Pathogenic Factor More Than a Biomarker." *International Journal of Molecular Sciences* 24(11): 9605.
- MIT Sloan. 2020. "5G, Explained.", Accessed 07.11.2024. https://mitsloan.mit.edu/ideas-made-to-matter/5g-explained
- Morris, H. R., M. G. Spillantini, C. M. Sue, and C. H. Williams-Gray. 2024. "The Pathogenesis of Parkinson's Disease." *Lancet (London, England)* 403(10423): 293–304
- STEMCELL Technologies. 2024. "mTeSR™1", Accessed 25.11.2024. https://www.stemcell.com/products/mtesr1.html
- Nelson, M. M., J. D. Hoff, M. L. Zeese, and G. Corfas. 2021. "Poly (ADP-Ribose) Polymerase 1 Regulates Cajal—Retzius Cell Development and Neural Precursor Cell Adhesion." *Frontiers in Cell and Developmental Biology* 9: 693595.
- Park, H., T. I. Kam, T. M. Dawson, and V. L. Dawson. 2020. "Poly (ADP-Ribose) (PAR)-Dependent Cell Death in Neurodegenerative Diseases." *Int Rev Cell Mol Biol* 353: 1–29.
- Pazzaglia, S., and C. Pioli. 2019. "Multifaceted Role of PARP-1 in DNA Repair and Inflammation: Pathological and Therapeutic Implications in Cancer and Non-Cancer Diseases." *Cells* 9(1): 41
- Schmid, M. R., S. P. Loughran, S. J. Regel, M. Murbach, A. B. Grunauer, T. Rusterholz, A. Bersagliere, N. Kuster, and P. Achermann. 2012. "Sleep EEG Alterations: Effects of Different Pulse-Modulated Radio Frequency Electromagnetic Fields." *Journal of Sleep Research* 21(1): 50–58.
- Schuermann, D., and M. Mevissen. 2021. "Manmade Electromagnetic Fields and Oxidative Stress—Biological Effects and Consequences for Health." *International Journal of Molecular Sciences* 22(7): 3772.
- Senturk, F., S. Cakmak, I. C. Kocum, M. Gumusderelioglu, and G. G. Ozturk. 2022. "Effects of Radiofrequency Exposure on in Vitro Blood-Brain Barrier Permeability in the Presence of Magnetic Nanoparticles." Biochemical and Biophysical Research Communications 597: 91–97.
- Stefi, A. L., L. H. Margaritis, A. S. Skouroliakou, and D. Vassilacopoulou. 2019. "Mobile Phone Electromagnetic Radiation Affects Amyloid Precursor Protein and α -Synuclein Metabolism in SH-SY5Y Cells." *Pathophysiology* 26(3–4): 203–12.
- Teleanu, D. M., A. G. Niculescu, I. I. Lungu, C. I. Radu, O. Vladâcenco, E. Roza, B. Costăchescu, A. M. Grumezescu, and R. I. Teleanu. 2022. "An Overview of Oxidative Stress, Neuroinflammation and Neurodegenerative Diseases." *International Journal of Molecular Sciences* 23(11): 5938.
- Thapa, K., H. Khan, U. Sharma, A. K. Grewal, and T. G. Singh. 2021. "Poly (ADP-Ribose) Polymerase-1 as a Promising Drug Target for Neurodegenerative Diseases." *Life Sci* 267: 118975.
- Thomas, Selina. 2023. "The Role of RF-EMF (5G) on Neuronal Development and Neuronal Health Using Brain Organoids." University of Bern.
- Wang, Y., Y. Zhang, S. Zhang, B. Kim, V. L. Hull, J. Xu, P. Prabhu, et al. 2021. "PARP1-Mediated PARylation Activity Is Essential for Oligodendroglial Differentiation and CNS Myelination." *Cell Rep* 37(1): 109695.
- Weber, M. B. M. 2023. "NogoA, a Player in Neurodegenerative Diseases? Characterization of Human IPSC-Derived NogoA Knockout Midbrain Neurons." University of Bern.

- WHO. 2020. "Radiation: 5G mobile networks and health" Accessed 27.11.2024.

 https://www.who.int/news-room/questions-and-answers/item/radiation-5g-mobile-networks-and-health
- Zhao, H., S. Wang, and X. Li. 2022. "DNA Damage Accumulation in Aging Brain and Its Links to Alzheimer's Disease Progression." *Genome Instability & Disease* 3(3): 172–78.
- Zhao, R., S. Zhang, Z. Xu, L. Ju, D. Lu, and G. Yao. 2007. "Studying Gene Expression Profile of Rat Neuron Exposed to 1800 MHz Radiofrequency Electromagnetic Fields with CDNA Microassay." *Toxicology* 235(3): 167–75.

Acknowledgements

I would like to sincerely thank Prof. Dr. Meike Mevissen for the opportunity to conduct my dissertation project in the Department of Veterinary Pharmacology and Toxicology in Bern, as well as for her invaluable guidance, support, and evaluation of my thesis, which were crucial for its completion. I am deeply grateful to Dr. Angélique Ducray and Dr. Rouaa Ben Chaabene for helping me to work with stem cells, providing constructive advice in planning and performing experiments, and critically evaluating my results, which significantly enhanced the quality of my research. I also want to thank the entire research team, including Azam Jamaati, Sara Alonso Jiménez, Daria Tschudin, Lea Walther and Alina Bähler, for their support, advice, and assistance in troubleshooting throughout my experiments.

Declaration of Independence

Ich, erkläre hiermit, dass ich die vorliegende Dissertation selbständig verfasst habe und keine anderen als die angegebenen Quellen benutzt habe. Alle Stellen, die wörtlich oder sinngemäss aus Quellen entnommen wurden, habe ich als solche gekennzeichnet.

Mir ist bekannt, dass andernfalls der Senat gemäss Artikel 36 Absatz 1 Buchstabe r des Gesetzes über die Universität vom 5. September 1996 und Artikel 69 des Universitätsstatuts vom 7. Juni 2011 zum Entzug des Doktortitels berechtigt ist. Für die Zwecke Begutachtung der Überprüfung der Einhaltung der und Selbständigkeitserklärung bzw. der Reglemente betreffend Plagiate erteile ich der Universität Bern das Recht, die dazu erforderlichen Personendaten zu bearbeiten und Nutzungshandlungen vorzunehmen, insbesondere die Dissertation zu vervielfältigen und dauerhaft in einer Datenbank zu speichern sowie diese zur Überprüfung von Arbeiten Dritter zu verwenden oder hierzu zur Verfügung zu stellen.

Bern, 26.11.2024

Alexander Baumgartner

Egyl.